5-2015

The Unusual Temporal and Spatial Slip History of the Wassuk Range Normal Fault, Western Nevada (USA): Implications for Seismic Hazard and Walker Lane Deformation

Benjamin E. Surpless
Trinity University, bsurples@trinity.edu

Glenn C. Kroeger
Trinity University, gkroeger@trinity.edu

Repository Citation

Surpless, B., & Kroeger, G. (2015). The unusual temporal and spatial slip history of the Wassuk range normal fault, western Nevada (USA): Implications for seismic hazard and walker lane deformation. *Bulletin of the Geological Society of America, 127*(5-6), 737-758. doi: 10.1130/B31159.1

The unusual temporal and spatial slip history of the Wassuk Range normal fault, western Nevada (USA): Implications for seismic hazard and Walker Lane deformation

B. Surpless[†] **and G. Kroeger**
Department of Geosciences, Trinity University, One Trinity Place, San Antonio, Texas 78212, USA

ABSTRACT

We document temporal and spatial variations in vertical displacement rate across 6 temporal orders of magnitude to better understand how the 100-km-long, east-dipping Wassuk Range normal fault system has accommodated strain in the context of the Walker Lane, a tectonically active, NNW-trending zone of dextral and extensional deformation that affects significant portions of western Nevada and eastern California. We combine ^{10}Be and ^{26}Al cosmonuclide exposure ages with shallow seismic and gravity data from the buried hanging wall of the Wassuk fault to derive a post–113 ka (10^5 yr time scale) vertical displacement rate of 0.82 ± 0.16 mm/yr. We also perform large-scale fault scarp analysis to constrain the long-term (>1 Ma; 10^6 yr time scale) displacement rate. Our fault-scarp analysis results imply similar vertical displacement rates, with higher long-term vertical displacement rates along the southern fault (~1.1 mm/yr) relative to the northern fault (<0.8 mm/yr).

Vertical displacement rate data at the 10^6, 10^5, 10^3, and 10^1 yr time scales (this study and others) support a constant vertical displacement rate between 0.75 and 1.0 mm/yr for the Wassuk Range fault since ca. 4 Ma. An anomalously high vertical displacement rate at the 10^4 yr time scale is best explained by an earthquake cluster between ca. 15.5 ka and ca. 10.5 ka, potentially linked to rapid filling of the Walker Lake basin immediately prior to the ca. 13 ka Sehoo highstand of ancestral Lake Lahontan. We hypothesize that this flood event induced seismicity by placing an additional load on the hanging wall of the Wassuk Range fault and by increasing the pore-fluid pressure within and adjacent to the fault. Although an earthquake cluster like this is consistent with Wallace-type fault behavior, we suggest that a nontectonic stressor induced the cluster, resulting in the apparent discrepancy in vertical displacement rate at the 10^4 yr time scale. Thus, we posit that the long-term slip along Wassuk fault is better explained by slip-predictable Reid-type behavior, which deviates from the behavior of other well-documented fault systems. Based on these results, we suggest that similar, unrecognized nontectonic stressors may influence rates of strain release along other major fault systems worldwide. Finally, we present a revised model of central Walker Lane kinematics, based on data from this and other recent studies.

INTRODUCTION

The advent of recent technological advances, such as terrestrial cosmogenic nuclide (TCN) geochronology, increasingly accurate geodetic information, and improved geophysical modeling tools, has enhanced our ability to compare strain accumulation and release across fault zones over a more complete range of time scales (e.g., Gosse and Phillips, 2001; Bennett et al., 2003; Friedrich et al., 2003; Grosfils et al., 2003; Foy et al., 2012). These temporal and spatial data permit us to address how fault behavior varies in areas of active tectonic deformation. Although strain rates across major plate boundaries appear to remain relatively constant over time (e.g., DeMets et al., 1994; Sella et al., 2002; Wallace et al., 2004; Cowgill et al., 2009), many studies have documented temporal changes in slip rate for smaller fault zones within larger zones of deformation (e.g., Wong and Olig, 1998, and references therein; Wong et al., 2002, 2004; Friedrich et al., 2003; Hoeft and Frankel, 2010; Olig et al., 2011; Rood et al., 2011). Few studies have evaluated changes in fault slip rate at time scales ranging from 10^1 to 10^5 yr (e.g., Rood et al., 2011); by constraining fault slip rate over the most complete range of time scales, we can better reconstruct behavior of a fault over time and define the role of that fault in accommodating strain within a broad zone of deformation. When compared with other major, well-documented fault systems worldwide, we might also develop a transferable model for fault behavior that improves the assessment of seismic hazard.

The Wassuk Range fault is a 100-km-long, east-dipping normal fault with one of the highest slip rates in the Basin and Range Province (Fig. 1; e.g., dePolo and Anderson, 2000). The fault helps accommodate deformation within the actively deforming Walker Lane–Eastern California shear zone, a zone of complex and evolving transtensional strain on the western margin of the Basin and Range Province (Fig. 1). This belt of deformation takes up a significant portion of the differential motion between the Pacific and North American plates (e.g., Hearn and Humphreys, 1998; Thatcher et al., 1999; Dixon et al., 2003; Bennett et al., 2003; Hammond and Thatcher, 2007; Kreemer et al., 2009; Hammond et al., 2011) and is complicated by a complex right step that kinematically links dextral deformation in the northern Eastern California shear zone (south of the Mina deflection) to the dextral faults in Walker Lane to the north (WLDF in Fig. 1), east of the Wassuk Range fault (e.g., Oldow et al., 2001, 2008; Hoeft and Frankel, 2010; Fig. 1). The position of this right stepover is thought to be controlled by crustal structure developed prior to the Tertiary (e.g., Oldow et al., 1989, 2008; Burchfiel et al., 1992) and possibly also explains the partitioning of strain between extensional-dominated deformation on the west and dextral deformation to the east at the latitude of the Wassuk Range (e.g., Oldow et al., 2001, 2008; Surpless, 2008; Fig. 1).

The Wassuk Range fault is considered to be the approximate boundary between these zones of dextral and extensional deformation in the

[†]bsurples@trinity.edu

GSA Bulletin; doi: 10.1130/B31159.1; 13 figures; 3 tables.

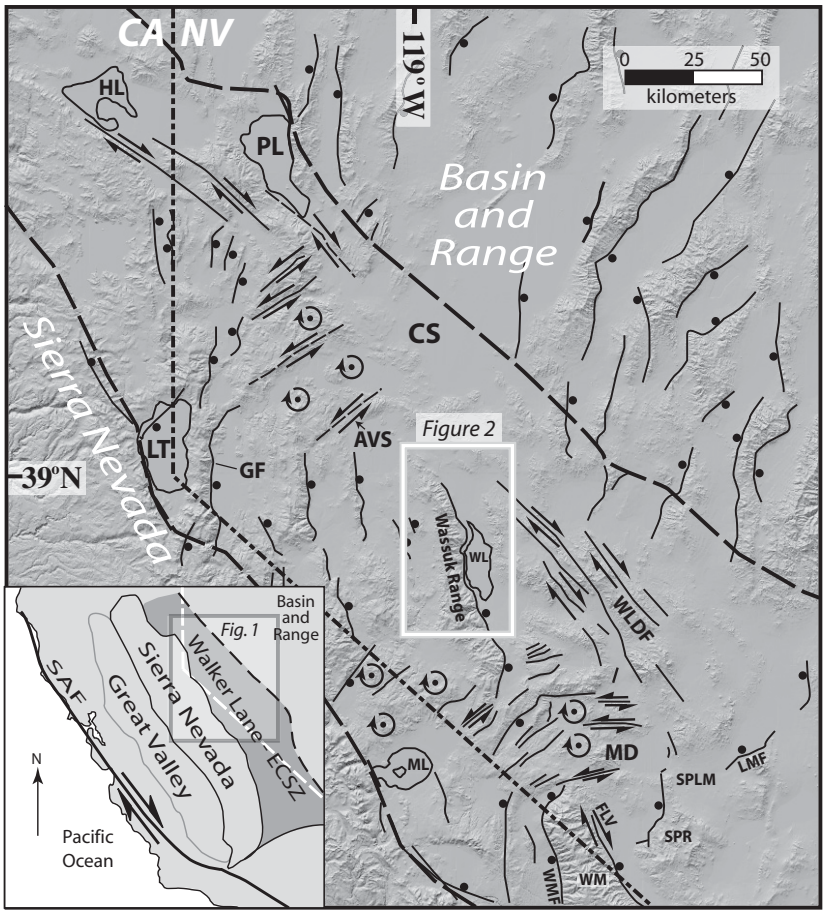

Figure 1. Digital shaded relief map and location map of the central and northern Walker Lane showing major normal faults, strike-slip faults, and crustal block rotations. Sense of motion is indicated on all faults, and positions of block rotations are indicated with a black dot and circle. The region shown in Figure 2 is boxed in white. The bold, black, dashed lines indicate the boundaries of the Walker Lane as delineated by Stewart (1988). Abbreviations: AVS—Adrian Valley sill; CS—Carson Sink; ECSZ—Eastern California shear zone; FLV—Fish Lake Valley fault; GF—Genoa fault; HL—Honey Lake; LMF—Lone Mountain fault; LT—Lake Tahoe; MD—Mina deflection; ML—Mono Lake; PL—Pyramid Lake; SAF—San Andreas fault; SPLM—Silver Peak–Lone Mountain extensional complex; SPR—Silver Peak Range; WL—Walker Lake; WLDF—Walker Lane dextral fault complex; WM—White Mountains; and WMF—White Mountains fault. Figure is modified after Stewart (1988); Ichinose et al. (1998); Surpless (2008); Lee et al. (2009); Hoeft and Frankel (2010); and Carlson et al. (2013).

Walker Lane (e.g., Oldow et al., 2001; Wesnousky, 2005; Surpless, 2008; Murphy et al., 2009; Wesnousky et al., 2012; Dong et al., 2014). The impressive topographic relief along the fault zone and previous geologic studies have established that displacement along the fault zone has been characterized by significant normal displacement across all time scales during Tertiary and Quaternary time (e.g., Dilles, 1993; Stockli et al., 2002; Surpless et al., 2002; Wesnousky, 2005; Surpless, 2011; Bormann et al., 2012; Wesnousky et al., 2012; Dong et al., 2014). Thus, the Wassuk Range fault system is ideal for an investigation of long-term variation in vertical displacement rates at a critical position within the broader Walker Lane–Eastern California shear zone.

Friedrich et al. (2003) studied the Wasatch fault system on the actively deforming eastern margin of the Basin and Range Province and documented significantly different vertical displacement rates on the fault at different observed time scales, with low rates of strain on the 10^5 yr time scale relative to strain rates during the Holocene (10^4 yr time scale). They attributed this difference to relatively low, uniform strain accumulation on long (10^5 yr or longer) time scales, with significantly higher rates of slip most likely associated with earthquake clustering on the 10^4 yr time scale. This study is consistent with many other studies (e.g., Wallace, 1987; Sieh et al., 1989; Grant and Sieh, 1994; Marco et al., 1996; McCalpin and Nishenko, 1996; Wong and Olig, 1998; Rockwell et al., 2000) that have suggested that temporal earthquake clustering along a fault zone results in records of greater or lesser slip rate at different time scales, depending on the time period recorded relative to the timing of these clusters.

In addition to establishing changes in slip rate over time, spatial variations and patterns of fault slip across the region are important to understanding the role of the Wassuk Range within the Walker Lane–Eastern California shear zone system. Rood et al. (2011) studied the Sierran frontal fault zone from the northern Eastern California shear zone (near the southern boundary of Fig. 1) into the Walker Lane at the latitude of Lake Tahoe, revealing both spatial and temporal changes in slip rate from ca. 150 ka to the present (Fig. 1). Their results suggest that between ca. 150 ka and ca. 20 ka, mean slip rates along strike of the Sierran frontal fault zone remained relatively constant on the same faults, at ~0.3 mm/yr and 0.4 mm/yr (Rood et al., 2011). However, Rood et al. (2011) documented significant variability on the same faults since ca. 20 ka, with slip rates increasing to the north along the Sierran frontal fault system, from ~0.3 mm/yr near the southern extent of Figure 1, where extension is shared with other faults such as the White Mountains and Fish Lake Valley faults, to 0.7 mm/yr on the fault that bounds the western edge of Mono Lake (Fig. 1). North of Mono Lake, these rates decrease rapidly to only 0.2 mm/yr along faults at the latitude of the southernmost Wassuk Range fault system and to only 0.3 mm/yr in faults associated with the Tahoe Basin (Fig. 1). Rood et al. (2011) suggested that much of the extensional strain must be transferred eastward north of the Mina deflection further north within the Walker Lane, coincident with the right step at the Mina deflection. These results suggest that the Wassuk Range might now accommodate a greater percentage of the total extensional deformation across the Walker Lane at this latitude.

Vertical displacement rates have been constrained for the Wassuk Range normal fault system since post-Pliocene time (10^6 yr time scale; Stockli et al., 2002; Surpless, 2011), late Pleistocene time (10^4 yr time scale; Dong et al., 2014),

and Holocene time (10^3–10^4 yr time scale; Bormann et al., 2012). In addition, Wesnousky et al. (2012) analyzed geodetic data to constrain modern rates of vertical displacement rate along the fault system (10^1 yr time scale). In this study, we use new geologic data, terrestrial cosmogenic nuclide (TCN) age data, shallow seismic data, gravity data, and large-scale fault scarp analysis (using the numerical modeling results of Petit et al., 2009a, 2009b) to construct a more complete record of vertical displacement rate over 6 temporal windows ranging from 10^6 yr to 10^1 yr. These data permit us to develop a model of time-dependent strain release for the Wassuk Range fault system, to compare the behavior of the fault to other major fault systems, and to assess the role of the Wassuk Range fault system within the actively deforming Walker Lane–Eastern California shear zone.

BACKGROUND

Temporal Variations in Displacement Rate and Models of Seismic Strain Release

On the eastern margin of the Basin and Range Province, Friedrich et al. (2003) used previous studies and new data to develop a displacement rate history for the Wasatch fault. Their work showed that time-averaged rates of displacement slowed over long time scales, from 1.0–1.4 mm/yr between 10 and 6 Ma to 0.2–0.3 mm/yr since 6 Ma (Friedrich et al., 2003). However, while the estimated time-averaged displacement rate of the fault was relatively low (<0.6 mm/yr) since 130 ka, the slip rate since 6 ka was significantly higher, at 1.7 ± 0.5 mm/yr. To explain the significantly higher rates of displacement in the Holocene, Friedrich et al. (2003) suggested the likelihood of earthquake clustering on the 10 k.y. time scale, with relatively low, uniform strain accumulation rates on the 100 k.y. time scale. Based on these results and on previous studies, they suggested that significant changes in displacement rate might be expected at the 10^6 yr scale (changes in tectonic loading; e.g., Atwater and Stock, 1998; Wernicke and Snow, 1998; Sonder and Jones, 1999), the 10^4 yr scale (clustered seismic strain release; e.g., Rockwell et al., 2000), and the 10^2 or 10^1 yr scale (postseismic transients; e.g., Hager et al., 1999; Savage, 2000; Dixon et al., 2003), thus implying that measurements of strain accumulation and release are time scale–dependent for any individual fault system.

Reid (1910) was the first to propose a model for seismic strain release, where elastic strain energy accumulates across locked faults and is released by earthquakes with relatively similar total slip and recurrence interval. This model was later modified to take into account that neither recurrence interval nor the size of earthquakes on a given fault is as regular as predicted (e.g., Shimazaki and Nakata, 1980). The resulting primary models that have been proposed to explain seismic strain release over time for a given fault system (e.g., Wallace, 1987; Ward, 1998; Friedrich et al., 2003) include slip-predictable behavior (time since the last earthquake predicts the magnitude of the next earthquake; e.g., Shimazaki and Nakata, 1980; Lay and Wallace, 1995), time-predictable behavior (the magnitude of the last earthquake predicts the time of the next earthquake; e.g., Shimazaki and Nakata, 1980), and clustered strain release behavior (long-term strain accumulation is accommodated primarily by clusters of earthquakes over short periods with long periods of relative quiescence; e.g., Wallace, 1987). All three models assume a relatively constant rate of far-field strain accumulation, suggesting that if displacement histories can be constrained over a long enough time period (i.e., over several earthquake cycles or clusters), documented slip rates should agree with modern (geodetic) measurements of far-field strain rate (e.g., Friedrich et al., 2003).

However, at many locations across the western United States, significant discrepancies exist between geodetic and geologic data (e.g., Friedrich et al., 2003; Lee et al., 2001; Oldow, 2003; Oskin et al., 2007; Rood et al., 2011; Wesnousky et al., 2012), highlighting the difficulty in developing robust models for the geologic evolution of a region, such as the Walker Lane–Eastern California shear zone, in the context of modern strain rates. Importantly, mismatch of geodetic and geologic data can be strongly affected by the timing of data collection relative to the longer-term seismic history of a given fault or system of faults. As summarized in Rood et al. (2011), mismatches might arise due to (1) the clustering of past earthquakes (e.g., Rockwell et al., 2000), resulting in an overestimate of geologic strain release rates; (2) geologic deformation accommodated by undetected structures (e.g., Sheehan, 2007), resulting in an underestimate of geologic strain release rates; or (3) geodetic sampling early in the interseismic cycle (e.g., Peltzer et al., 2001; Dixon et al., 2003), resulting in geodetic strain rates that are higher than the average interseismic rate (e.g., when geodetic sampling measures viscoelastic relaxation). Importantly, some slip rate variations have been shown to record coordination of strain between neighboring fault systems (e.g., Lee et al., 2009; Petronis et al., 2009; Nagorsen-Rinke et al., 2013) as opposed to the timing of data collection relative to seismic events. Thus, when evaluating temporal and spatial changes in vertical displacement rates for the Wassuk Range fault, we will need to account for the potential impacts of one or more of these factors in our interpretation of deformation in the context of the Walker Lane–Eastern California shear zone system.

In addition, Chang et al. (2006) demonstrated that the method of calculation of vertical strain rates from horizontal geodetic data could account for some of the discrepancies between geologic and geodetic strain rates. Their work suggests that vertical strain rate values calculated from geodetically derived horizontal strain rates across any major fault are strongly affected by both subsurface fault geometry and the angle of simple shear experienced by the hanging wall during normal-fault rupture events. They evaluated rates of strain loading (geodetic data) and release (geologic data) across the Wasatch fault using a finite strain model for normal-fault rupture developed by White et al. (1986). Their results indicate that in past studies where only fault dip was taken into account (e.g., Friedrich et al., 2003), it is likely that vertical strain rates calculated from horizontal geodetic strain rates were too high (Chang et al., 2006).

Walker Lane–Eastern California Shear Zone Deformation

The Wassuk Range lies within the Walker Lane–Eastern California shear zone, a zone that accommodates ~25% of the dextral strain associated with the North American–Pacific plate boundary and also accommodates extension related to classic Basin and Range deformation (e.g., Argus and Gordon, 1991; Dixon et al., 1995; Bennett et al., 2003; Kreemer et al., 2009). At ~38°N latitude, the slip from dextral faults of the Eastern California shear zone is transferred east through the Mina deflection, where a combination of clockwise crustal block rotations, normal faults, sinistral faults, and minor thrust faults (e.g., Oldow, 2003; Lee et al., 2009; Petronis et al., 2009) accommodates the northward transition into the Walker Lane. Importantly, Rood et al. (2011) suggested that extensional deformation, since ca. 20 ka, has also been transferred eastward from the northern Eastern California shear zone to the Walker Lane, with very low slip rates recorded along the Sierran frontal fault zone north of the Mina deflection (Fig. 1).

Recent geodetic studies have revealed that right-lateral strain accumulation across the width of the Walker Lane is on the order of 6–7 mm/yr at the latitude of the Wassuk Range (e.g., Wesnousky et al., 2012; Dong et al., 2014). Although geodetic data suggest broad accommodation of transtensional strain in the

Walker Lane (e.g., Bennett et al., 2003; Hammond et al., 2011), geologic evidence suggests that deformation is strongly partitioned into a zone of shear-dominated strain to the east and extension-dominated strain to the west (e.g., Oldow, 2003; Wesnousky, 2005; Surpless, 2008), with several workers suggesting that the Wassuk Range is the approximate present-day boundary between these zones (e.g., Oldow et al., 2001; Wesnousky, 2005; Surpless, 2008; Murphy et al., 2009). Although Dong et al. (2014) recently identified an active right-lateral strike slip fault in the northern Wassuk Range (DSS in Fig. 2), their work suggests that most, if not all, dextral deformation is accommodated outboard (east) of the range-bounding normal fault, within the Walker Lake basin. However, Hammond et al. (2011) and Wesnousky et al. (2012) posited that some oblique motion may occur along the Wassuk Range fault. The transition between the Sierra Nevada and the Walker Lane at the latitude of Lake Tahoe consists of a series of left-stepping, en echelon normal faults, including the Genoa fault and the Wassuk Range fault, all of which display evidence for normal faulting without significant dextral deformation (e.g., Dilles, 1993; Cashman and Fontaine, 2000; Oldow et al., 2001; Wesnousky, 2005; Fig. 1).

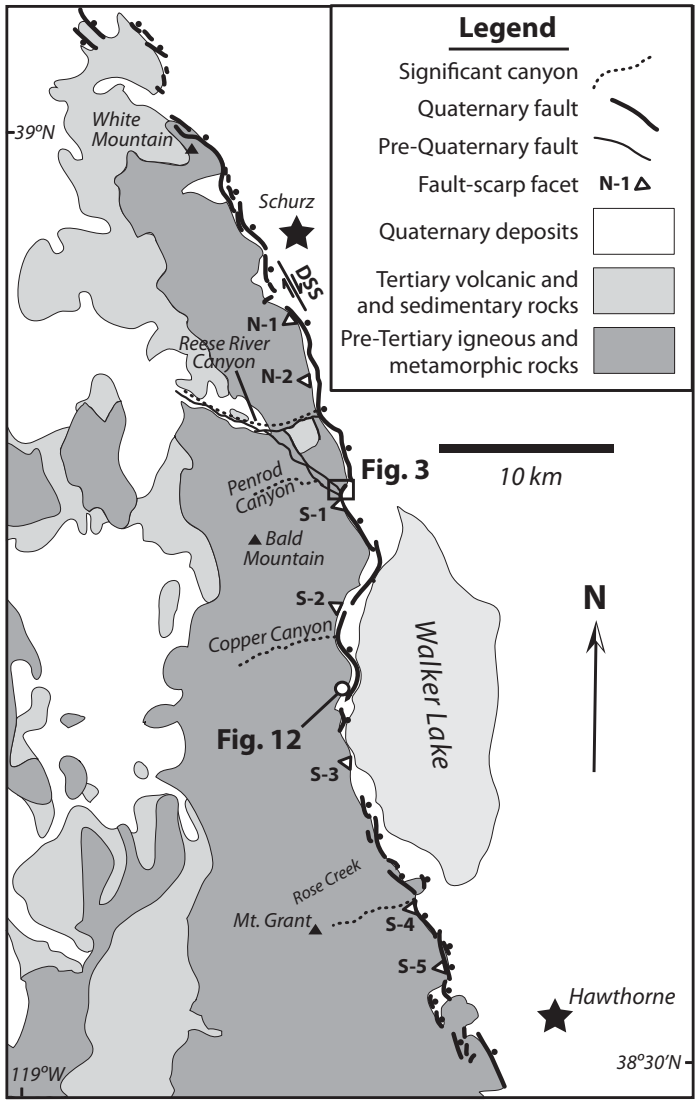

Figure 2. Map of the Wassuk Range with Quaternary range-front faults and pre-Quaternary faults adjacent to Penrod Canyon highlighted. Note the right step in the range-front fault system at the latitude of Penrod Canyon. Locations of Figures 3 and 12 are indicated. Triangular fault-scarp facets used in slip-rate estimates are indicated by white triangles. Dextral strike-slip fault identified by Dong et al. (2014) is indicated by DSS, to the south of the town of Schurz. Map is significantly modified from: Stewart and Carlson (1978); Ludington et al. (1996); Wesnousky (2005); and Surpless (2010a, 2010b).

To help explain the right-lateral shear identified to the west of the Wassuk Range by geodetic data, Wesnousky et al. (2012) suggested that this dextral strain is accommodated in part by crustal block rotations about a vertical axis, with major normal faults across the Sierra Nevada–Walker Lane transition accommodating primarily dip-slip motion. Similarly, Carlson et al. (2013) studied the evolution of faults and crustal blocks to the west of the southern Wassuk Range, within the Sierra Nevada–Walker Lane transition zone north of Mono Lake, where they documented significant (~30°) clockwise rotation of crustal blocks since late Miocene time, helping explain the lack of significant dextral strike-slip faults to the west of the Wassuk Range fault system (Fig. 1).

However, recent studies have shown that crustal block rotations between the Wassuk Range and the Lake Tahoe region do not account for all geodetically determined dextral shear (e.g., Hammond et al., 2011, 2012; Bormann, 2013). Hammond et al. (2012) analyzed the velocity field across the Lake Tahoe Basin, from the Sierran range crest on the west to the Carson Range on the east (Fig. 1), and determined that the Tahoe Basin is actively accommodating dextral motion associated with the Pacific–North American plate boundary. In addition, although difficult to detect with geologic studies and not evident in historical earthquake records (e.g., Surpless, 2008, and references therein), it is possible that an additional component of dextral shear is taken up within basins between the Wassuk Range and Lake Tahoe (Hammond et al., 2011; Wesnousky et al., 2012; Bormann, 2013; Fig. 1). Thus, although geologic data suggest that no significant dextral shear has been accommodated to the west of the Wassuk Range, analyses of geodetic data indicate that some portion of ongoing dextral deformation must be accommodated across the entire width of the Walker Lane at this latitude. In our analysis of the Wassuk Range fault, we focus on vertical displacement associated with the steeply dipping range-front fault, assuming that most past deformation along the fault system has been primarily dip slip; however, we cannot discount the possibility that some component of dextral deformation has been accommodated along the fault system.

Geologic History of the Wassuk Fault System

Immediately south of Penrod Canyon (Fig. 2), large-magnitude, ENE-WSW–directed extension event (>150%) was accommodated by ENE-dipping, high-angle normal faults spaced at 1–2 km intervals starting at ca. 15 Ma (Surpless, 2010a, 2011). The timing of the onset of extension is based on both crosscutting relationships and low-temperature thermochronologic data (Surpless et al., 2002; Stockli et al., 2002; Surpless, 2011); these data also suggest that this period of elevated extensional strain ended by ca. 13 Ma (Stockli et al., 2002; Surpless, 2011). During this same period in the northern Wassuk Range, Dilles (1993) documented a series of strike-slip faults that moved synchronously with oblique-slip normal faults to accommodate an average of 50° stratal rotation of fault blocks, with a dominant extension directed WNW-ESE to NW-SE. Although the pre-Quaternary NW-striking fault system adjacent to the Penrod Canyon–Reese River Canyon area (Fig. 2) is subparallel to the most prominent dextral faults in the Walker Lane to the east of Walker Lake (Fig. 1), all strike-slip faults documented by Dilles (1993) were largely accommodation structures between zones of oppositely dipping normal faults and exhibit little lateral displacement. In the northern Wassuk Range, this period of elevated rates of extension ended by 14 Ma (Dilles, 1993).

Low-temperature thermochronologic data suggest that rates of footwall uplift related to extension remained low in the central Wassuk Range until ca. 4 Ma (Stockli et al., 2002). At that time, thermochronologic data suggest a renewed pulse of extension that has continued to the present, potentially related to a fundamental change in plate boundary dynamics (Surpless, 2011). Murphy et al. (2009) suggested a fundamental kinematic reorganization of the plate boundary at this time, based on their graphical inversion analysis of contemporary velocity and strain across the Walker Lane at this latitude. Stockli et al. (2002) constrained a time-averaged rate of footwall uplift at 0.5–0.75 mm/yr for the central Wassuk Range since 4 Ma (at the 10^6 yr time scale). Structural reconstructions and thermochronologic data imply that this uplift has been accommodated by the range-front fault system, which remains active today (Surpless et al., 2002; Stockli et al., 2002; Surpless, 2011).

Dong et al. (2014) utilized high-resolution seismic compressed high intensity radar pulse (CHIRP) profiles collected from Walker Lake to constrain vertical displacement rate on the 10^4 yr time scale on the Wassuk fault. They interpreted ca. 20 ka stratigraphy that has been tilted westward with a magnitude consistent with 1.0–1.5 mm/yr of vertical displacement along the primary range-bounding fault (Dong et al., 2014). In addition, Dong et al. (2014) documented a strike-slip fault subparallel to the range front but outboard of the dominant range-front fault system (DSS in Fig. 2), constraining dextral slip rate to 1 mm/yr since ca. 15.5 ka. Importantly, Dong et al. (2014) also documented significant folding of lake sediments older than ca. 10.5 ka, with younger sediments unaffected by deformation. If this folding is the assumed to be the result of deformation associated with fault activity, these findings suggest a possible cluster of earthquakes lasting no more than ~5 k.y., between ca. 15.5 ka and ca. 10.5 ka (Dong et al., 2014).

Based on well-exposed slip indicators (slickenlines and slickensides) in granitic bedrock along the central and northern Wassuk Range, the present-day maximum extension direction is approximately N75°W (Surpless, 2011). Some workers (e.g., Wallace, 1977; Demsey, 1987; Wesnousky, 2005) have considered the relatively simple morphology of abundant Holocene scarps exposed in drainages along much of the range front to imply a single-event origin for most parts of the Wassuk Range. Based on trenching, soil development, and fault scarp morphology, Demsey (1987) documented two significant earthquakes in the past 5000 yr along the range-front fault system, with 2–3 m of offset per event, and obtained a vertical displacement rate of 0.4–0.5 mm/yr based on her work. These two events affected different segments of the fault system: In the southern Wassuk Range, a single M 7.0–7.1 earthquake at ca. 4500 yr B.P. resulted in displacement along ~30 km of the range front, and along a segment further north, a single M 7.2–7.5 earthquake at ca. 2500 yr B.P. resulted in displacement along ~50 km of the range front, extending up to but not to the north of the abandoned Penrod Canyon alluvial fan (Demsey, 1987).

However, Bormann et al. (2012) used observations and age data from two trenches at the apex of the Rose Creek alluvial fan (Fig. 1) to establish that at least three significant seismic events have occurred since ca. 9400 cal. (calibrated calendar years) B.P., with the most recent displacement postdating ca. 2810 cal. B.P., perhaps as young as ca. A.D. 1850. These earthquakes resulted in ~7.0 m of total vertical offset, yielding a Holocene vertical displacement rate of 0.7 ± 0.1 mm/yr, i.e., higher than Demsey's (1987) estimate. This work also suggests that many of the apparent single-event Holocene scarps mapped along the range front (e.g., Demsey, 1987) may in fact be unrecognized multiple-event scarps (Bormann et al., 2012). Significantly, both of the Rose Creek study locations displayed apparent single-event scarp morphologies (Bormann et al., 2012); thus, we place higher confidence in the vertical displacement rate estimated by Bormann et al. (2012).

Recently, Wesnousky et al. (2012) used geodetic data to construct the modern strain fields local to the major fault systems across the Walker Lane at the latitude of Lake Tahoe. Their method avoided the effects of predefined crustal blocks, which are commonly used in geodetic modeling, thus permitting the estimation of fault-normal horizontal extension rates at the 10^1 yr time scale for individual faults (Wesnousky et al., 2012). Their calculated horizontal extension rates for the central section of the Wassuk fault (at the approximate latitude of Bald Mountain; Fig. 2) and the northern Wassuk fault (north of Reese River Canyon; Fig. 2) were 0.4–0.7 mm/yr and 0.9–1.0 mm/yr, respectively (Wesnousky et al., 2012). To convert these values from horizontal extension rate to vertical displacement rate, we assumed a range in fault dips between 45° and 60°, consistent with previous studies of the range-bounding fault (e.g., Dilles, 1993; Stockli et al., 2002; Surpless, 2010a, 2011; Bormann et al., 2012), and we calculated the vertical displacement rate using the equation:

$$v_{vert} = v_{hor} \times \tan\theta, \quad (1)$$

where $v_{vert.}$ is vertical displacement rate, $v_{hor.}$ is horizontal extension rate, and θ is dip of the normal fault. The calculated vertical displacement rates for the central section of the Wassuk Range fault, at 0.4–1.2 mm/yr, and for the northern section, at 0.9–1.7 mm/yr, are consistent with most vertical displacement rates determined at other time scales for the range-bounding fault.

Penrod Canyon Pediment

At the mouth of Penrod Canyon (Fig. 2) in the northern Wassuk Range, a large, abandoned and dissected alluvium-covered bedrock pediment displays a well-defined escarpment striking approximately N30°E at a right step in the NNW-striking range-front fault system (Figs. 2 and 3). The intact central section of the Penrod Canyon pediment is separated by two active creek systems, which have eroded downward through the pediment, separating the central pediment from smaller sections of the alluvium-covered surfaces to the northeast and southwest (Fig. 3). The NE-trending escarpment displays eroded wave-cut benches with fluvial and lacustrine pediment deposits (Qflp in Fig. 3) created during a late Pleistocene lake-level highstand of ancestral Lake Lahontan at ca. 13 ka (Sehoo highstand; Adams and Wesnousky, 1998), and

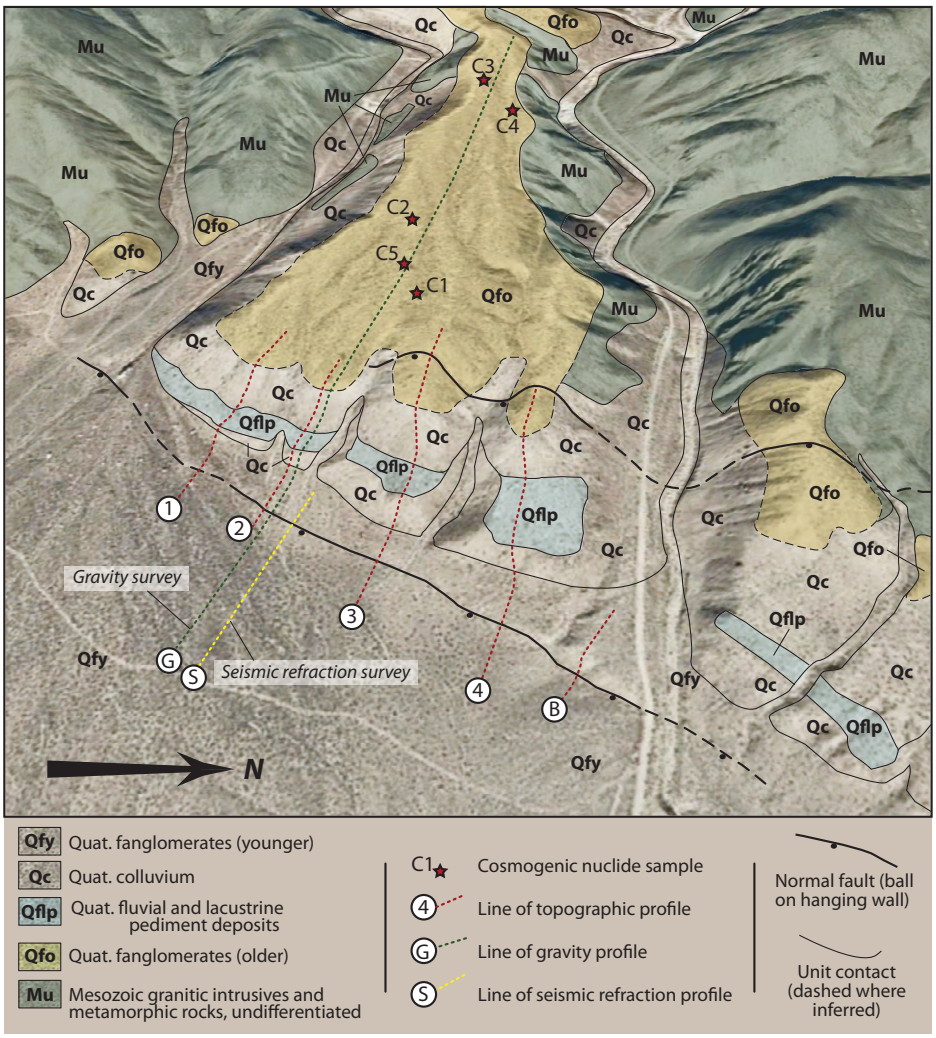

Figure 3. Oblique view of the dissected Penrod Canyon pediment system. Stars indicate cosmonuclide sample positions; fine black lines indicate contacts between units; bold black lines indicate faults (dashed where inferred); red dashed lines indicate lines of profile (shown in Fig. 5); yellow dashed line indicates position of seismic-refraction survey (results shown in Fig. 9); and green dashed line indicates position of gravity survey (results shown in Fig. 10). Profile B is from Bormann et al. (2012). Figure is significantly modified from House and Adams (2009) and Surpless (2010b). Length of seismic refraction survey line is 200 m. Background image is from Google Earth.

well-preserved Holocene fault scarps subparallel and proximal to the base of the escarpment suggest that this segment of the range-bounding fault system remains active today (Fig. 3; Wesnousky, 2005; Bormann et al., 2012). To our knowledge, the abandoned Penrod Canyon pediment is the only such exposure along the Wassuk Range front with good, laterally extensive exposures of the contact between Mesozoic intrusive units and older, inactive Quaternary alluvium (Qfo; Fig. 3).

Importantly, Bormann et al. (2012) estimated the depositional age of the inactive, upper alluvial surface (Qfo) at 112.9 ± 12.5 ka. Although Bormann et al. (2012) used this age to estimate the rate of vertical displacement along the Wassuk Range front fault system at Penrod Canyon, the unknown thickness of alluvium in the hanging wall of the fault system prevented a well-constrained analysis of time-averaged vertical displacement rate since the abandonment of the pediment. Fortunately, the contact between Mesozoic bedrock (Mu) and the Quaternary alluvial deposit (Qfo), where buried in the fault system's hanging wall, provides an excellent velocity contrast for shallow seismic investigation and an excellent density contrast for gravity investigation.

METHODS

In this study, we use new geologic data, topographic profile surveys, cosmogenic nuclide exposure age dates, seismic refraction, and gravity data to provide a more complete picture of the fault system and more tightly constrain the rate of vertical displacement at the 10^5 yr time scale. We also use the faceted-spur analysis method developed by Petit et al. (2009a, 2009b) to provide another estimate of the long-term (>1 m.y.) vertical displacement rate for the range-front fault system. These two new slip rate estimates fill in important temporal gaps for the Wassuk Range fault system and permit us to better evaluate strain release over time.

Geologic Investigation and Topographic Profile Surveys

To constrain the spatial distribution and lithologic characteristics of rock units for our analysis of vertical displacement along the Wassuk fault, we performed new geologic mapping of the Penrod Canyon pediment. We used an integrated base map that included a digitized 1:24,000 U.S. Geological Survey (USGS) topographic map, high-resolution (25 pixels/m) orthophotos, and USGS digital elevation models. We logged spatial data using a Trimble GeoXH handheld global positioning system (GPS) receiver. We determined the spatial distribution of rock units in the field based on the lithologic characteristics and previous geologic maps (House and Adams, 2009; Surpless, 2010a). We augmented field descriptions and sketches with notated field photographs of important features.

We constructed topographic profiles perpendicular to the larger, older escarpment and the younger Holocene scarps (lines of profile shown as red, dashed lines in Fig. 3) to constrain both the minimum magnitude of vertical displacement for scarps of both ages as well as the number of events recorded by the Holocene scarps proximal to the older surfaces. The positions of these lines were chosen to best represent the most intact scarp profiles, avoiding areas of active scarp dissection by small drainages (Fig. 3), and we used a Leica TCR405 total station to measure position and elevation, with base stations GPS-located with a handheld Trimble GeoXH unit.

Cosmogenic Nuclide Exposure Age Dating

We utilized terrestrial cosmogenic nuclide (TCN) ^{10}Be and ^{26}Al exposure age dating to constrain the age of the abandoned depositional surface (Qfo) on the Penrod Canyon pediment, permitting us to calculate a postdepositional strain

rate at the 10^5 yr time scale. In cases where the age of a deposit is beyond the limit of radiocarbon dating (ca. 40 ka) and where datable organic material is nonexistent, the use of TCN dating techniques is the only viable method to determine the age of an alluvial surface (e.g., Hoeft and Frankel, 2010). In this study, we sampled three undated granitic boulders on the abandoned alluvial surface in order to better constrain the depositional age of the surface, originally dated by Bormann et al. (2012) at 112.9 ± 12.5 ka. We assume that the ages calculated for these samples correspond to the length of time these rocks have been exposed to cosmogenic radiation (e.g., Gosse and Phillips, 2001). The authors collected samples C3, C4, and C5 from these boulders (see sample locations on Fig. 3), targeting the largest boulders not yet sampled (samples C1 and C2 from Bormann et al. [2012] were sampled from the largest boulders on the alluvial surface). All samples were collected from apparently stable parts of the upper alluvial surface to avoid the effects of disturbance or recent exhumation.

Purdue Rare Isotope Measurement Laboratory (PRIME Laboratory of Purdue University) prepared and measured the amounts of ^{10}Be and ^{26}Al present (Sharma et al., 2000). Al_2O_3 and BeO were derived from the quartz portion of these granitic samples, using the methods described by Kohl and Nishiizumi (1992). The ^{26}Al and ^{10}Be exposure ages we report were calculated using version 2.2 of the CRONUS-Earth online exposure age calculator (Balco et al., 2008). We calculated ^{26}Al and ^{10}Be exposure ages assuming no erosion for each of the samples, using a constant production rate model (Lal, 1991; Stone, 2000).

Seismic Refraction

We collected seismic-refraction data in order to place constraints on sediment thickness in the hanging wall as a function of position relative to the documented pre-Holocene fault scarp. We used these data in combination with geologic mapping data from the footwall of the fault to constrain the total vertical displacement since fault formation. Importantly, the strong velocity and density contrasts between Mesozoic bedrock and Quaternary alluvium permit us to determine the depth to bedrock in the hanging wall, a value for which we have no other information. We selected a seismic survey line that was perpendicular to the scarp surfaces and that was adjacent to our chosen position for the gravity survey line (Fig. 3). Position of the seismic-refraction survey was also chosen to avoid the effects of the larger drainage systems to the northwest and southeast of the preserved pediment (Fig. 3).

We collected P-wave refraction data using a 24 channel Geometrics GEODE seismograph, 10 Hz geophones, and a sledgehammer energy source (12 lb. [5.4 kg] sledgehammer impacting a 6 in. [15.24 cm] square aluminum plate). Geophone spacing was 10 m along the 200-m-long survey line (Fig. 3). All resulting shot gathers show clear first-breaks at offsets of up to 100 m. As with topographic profile positions, we used a Leica TCR405 total field station to locate all geophone positions, with base station location established using a handheld Trimble GeoXH GPS unit. We suggest that depths derived from these data are accurate to approximately ±5 m.

Gravity

To complement seismic-refraction data, we chose a gravity survey line that was perpendicular to the scarp surfaces and adjacent to topographic profile 2 and the seismic-refraction survey (Fig. 3). We chose this location because it permitted us to measure gravity along the greatest possible distance along the upper alluvial surface (Qfo in Fig. 3). As with the seismic-refraction survey, position of the gravity survey line was also chosen to avoid the effects of the larger drainage systems to the northwest and southeast of the preserved pediment (Fig. 3). Gravity data permit us to better constrain the depth of sediment in the hanging wall of the fault as well as to estimate the dip of the unexposed fault plane.

We collected gravity data from 32 stations, with an approximate 20 m station spacing along the 700-m-long profile (Fig. 3), using a Lacoste and Romberg model gravimeter. All stations were established using a Leica TCR405 total field station; measurements were repeated at a gravity base station (GS1 or GS17) every 2 h or less to provide data for linear drift corrections, and all data were corrected for latitude, elevation, and topography using standard post-processing methods (e.g., Burger, 1992). We used free-air corrections as opposed to Bouguer modeling with terrain corrections because of the variable densities in the near surface as well as above gravity stations.

Faceted-Spur Analysis

To provide an estimate of vertical displacement rate along the Wassuk Range normal fault system at the >1 m.y. time scale, we applied the results of numerical modeling by Petit et al. (2009a, 2009b) to faceted spurs along the Wassuk Range normal fault system. Petit et al. (2009a) tested the sensitivity of climatic (diffusion coefficient, effective precipitation rate, and characteristic length scale) and tectonic (fault dip angle and slip rate) parameters upon the development of faceted spurs associated with major active normal faults. Surprisingly, their sensitivity tests suggest that a fault scarp will only bear faceted spurs when diffusion and incision processes balance, with the formation of these features not strongly controlled by climatic conditions (Petit et al., 2009a). In addition, the fault dip angle does not significantly control facet height or slope angle; these values are instead primarily controlled by the vertical displacement rate (Petit et al., 2009a, 2009b), an idea supported by the development of triangular facets on the spurs of the hanging walls of reverse faults (e.g., Bull, 2007). Petit et al. (2009a) pointed out that facet shape (including facet height) reaches a steady state by ca. 0.7–1.0 m.y., regardless of the duration of the experiment or variations in model erosion parameters, a finding that we can apply to facet development along the Wassuk Range fault. These results imply that the development of facets is most fundamentally controlled by base-level fall (e.g., Bull, 2007).

Using normal fault systems along the Wasatch Range (Utah, U.S.A.) and the Northern Baikal Rift (Russia), Petit et al. (2009a, 2009b) demonstrated that that the height of triangular faceted spurs along the footwalls of normal fault systems could be used as a proxy to determine the long-term (>1 m.y.) throw rates on these fault systems (Petit et al., 2009a, 2009b). Importantly, Petit et al. (2009a, 2009b) quantified strong linear correlations between mean facet height and mean facet slope as well as between mean facet height and throw rate.

We visually identified candidates for these calculations using Google Earth Professional (locations of spurs shown in Fig. 2). We evaluated the suitability of each facet based on the physical criteria outlined by Petit et al. (2009b), who suggested that spurs: should exhibit heights greater than 150 m; should show no evidence of significant landsliding on the scarp faces; and should not exhibit strong facet imbrication. We selected facet candidates that best matched those criteria, but in some cases, facet imbrication had affected spur morphology, so we chose the largest facet dimensions, as suggested by Petit et al. (2009b). Importantly, not all portions of the range front exhibited clear triangular facets, which might be caused by variations in bedrock strength (e.g., Ellis et al., 1999). The locations of the chosen facets are displayed on Figure 2.

We constructed topographic profiles along lines that intersected the upper apex of seven chosen spurs, were centered on each facet, and were perpendicular to the fault trace at that location (Fig. 4A). We then measured the difference in elevation between the position of

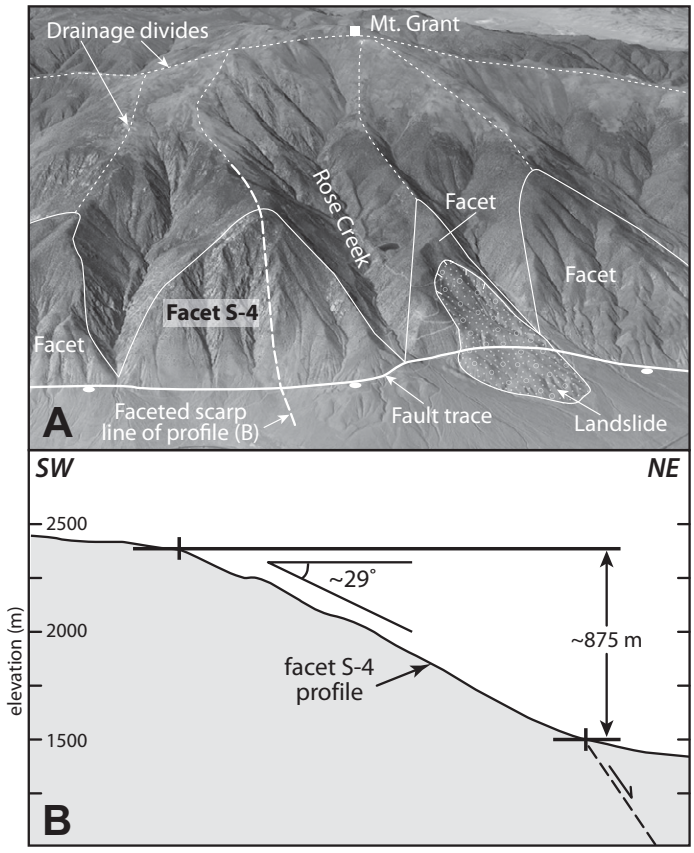

Figure 4. Example of triangular facet analysis, based on Petit et al. (2009a, 2009b). (A) Oblique view of triangular, facet-bearing scarps adjacent to the Wassuk range-bounding fault zone near Mount Grant, including facet S-4, used in this study. Image is from Google Earth, looking toward the southwest. See Figure 2 for location. (B) Facet-perpendicular profile, showing points used in calculation of facet height and angle.

the fault trace and upper apex of the exposed triangular facet to determine spur height, and the facet slope was measured perpendicular to the fault trace using these two points, following the method of Petit et al. (2009a) (Fig. 4B). We determined observational errors in these measurements (±10 m vertical; ±20 m horizontal) based on uncertainties in the positions of the fault trace and the crest of each faceted spur. Errors in slope angle are related to the positions of these two points, so positive and negative errors vary by facet. We also measured the height of the range crest adjacent to each spur. Finally, we used the linear relationship between facet height and vertical displacement rate (vertical displacement rate = 0.0013 × facet height), as determined by Petit et al. (2009a, 2009b), to estimate the vertical displacement rates of the Wassuk Range normal fault system for each measured facet. The errors included in Table 1 are based on the range in real-world calibration value relative to this theoretical linear relationship, shown in Figure 3A of Petit et al. (2009b), which is approximately ±0.20 mm/yr.

RESULTS

Geologic Investigation and Topographic Profiles at Penrod Canyon

Our geologic investigation of the Penrod Canyon pediment revealed important details about active alluvial processes that have affected exposure along the range-front fault system. The southwest creek system once fed an alluvial cone, which partially obscures sections of the Holocene scarps proximal to the larger, pre-Holocene pediment escarpment (Fig. 3). However, since that time, the creek has eroded through exposures of the Holocene scarp and is actively downcutting through this alluvial cone, with active deposition now taking place to the ESE, more than 1 km outside of the study area. Similarly, the creek system to the northwest of the central pediment is presently downcutting through young Quaternary alluvium (Qfy), with deposition occurring to the ESE, outside the study area. Smaller, headward-eroding drainage systems have cut through late Pleistocene fluvial and lacustrine platform veneer deposits (Qflp) adjacent to lines of profile 1, 2, and 3 (Fig. 3), and these smaller systems have established small, actively aggrading debris cones, which commonly obscure exposures of the Holocene scarp system to the ESE. The upper reaches of these small drainage systems also appear to be modifying the older alluvial surface (Qfo) to the WNW (Fig. 3).

Where the bedrock-alluvium contact is best exposed on the footwall of the fault, a weathered, coarsely crystalline Mesozoic quartz diorite (Mu) pediment is covered by a relatively thin (estimated at <3 m) layer of alluvium (Qfo; Fig. 3). The upper surface of Qfo dips ~4.5° toward the SE, toward the valley and perpendicular to the strike of the range-front fault. Since alluvial cover thicknesses are typically a few meters or less for the proximal reaches of pediment surfaces for 1 km or more valleyward (e.g., Cooke and Mason, 1973; Dohrenwend and Parsons, 1994), we suggest that the upper bedrock surface is likely similar to the ~4.5° dip value measured for the upper Qfo surface. The active alluvial surface (Qfy) valleyward of the uplifted pediment and Holocene fault scarps (Fig. 3) has a slope of 2.5°, which is shallower than the older alluvial surface (Qfo).

The total vertical displacements recorded by the larger escarpment at profiles 1 through 4 reveal values of ~45 m, ~40 m, ~47 m, and ~48 m, respectively, between the abandoned upper alluvial surface (Qfo) and the active alluvial surface (Qfy; Figs. 3 and 5). Profiles 1–4 (Fig. 5) reveal the eroded late Pleistocene wave-cut bench at approximately the same elevation (bold, black arrowheads on Fig. 5), with the shape of this bench at each profile likely affected by variations in the amount of erosion and colluvial deposition from the slope above. This variation in minimum displacement values parallel to the fault scarp is likely due to variations in the thickness of alluvial cover on the hanging wall, with the thickest cover adjacent to the alluvial cones with apices at several positions along the fault scarp (Fig. 3). Thus, the minimum vertical displacement since the upper alluvial surface was active is assumed to be ~48 m. Profile 3 also reveals a significant (7.0 m) vertical offset of the abandoned upper alluvial surface, northwest of the large escarpment (Fig. 5). The position of this offset is coincident with the fault identified by House and Adams (2009), shown

TABLE 1. PENROD CANYON BOULDER SAMPLE DATA

Sample name	Latitude (°N)	Longitude (°W)	Elevation (m)	Boulder height (m)	Sample thickness (cm)†	Horizon correction§	Measured ^{10}Be (×10^3 atoms /g quartz)#,**	^{10}Be minimum exposure age and 1σ analytical (internal) uncertainty (ka)††,§§,##	Model (external) uncertainty (k.y.)	Measured ^{26}Al (×10^3 atoms /g quartz)#,***	^{26}Al minimum exposure age and 1σ analytical (internal) uncertainty (ka)††,§§,##	Model (external) uncertainty (k.y.)	^{26}Al/^{10}Be ratio
C1*	38.8135	118.7794	1363	1.0	3	0.997	911.0 ± 20.5	75.7 ± 1.7	± 6.9	7133.0 ± 349.1	89.6 ± 4.6	± 9.3	7.83 ± 0.42
C2*	38.8136	118.7804	1370	1.5	4	0.997	1331.3 ± 31.2	111.9 ± 2.7	± 10.4	9250.6 ± 472.0	118.1 ± 6.4	± 12.6	6.96 ± 0.39
C3	38.8142	118.7832	1392	0.5	3	0.998	997.4 ± 16.9	73.3 ± 1.3	± 6.6	6705.5 ± 550.7	82.2 ± 7.0	± 10.2	6.72 ± 0.39
C4	38.8146	118.7825	1386	0.9	3	0.998	946.4 ± 22.6	69.8 ± 1.7	± 6.4	6215.1 ± 501.0	76.3 ± 6.4	± 9.4	6.57 ± 0.39
C5	38.8136	118.7799	1366	0.5	3	0.998	767.3 ± 19.0	57.2 ± 1.4	± 5.2	5052.5 ± 519.9	62.5 ± 6.6	± 8.7	6.58 ± 0.39

*Samples C1 and C2 (CWL1) from Bormann et al. (2012).
†Fraction corrected for finite sampling depth.
§Correction done according to Lal (1991).
#AMS (accelerator mass spectrometry) measurements performed at PRIME Laboratory following procedures described by Sharma et al. (2000).
**Samples referenced to 07KNSTD standard.
††Exposure age calculated using Cronus-Earth online exposure age calculator (Balco et al., 2008), version 2.2 (hess.ess.washington.edu/math/).
§§Age estimates based on a constant production rate model. Scaling done according to Stone (2000) after Lal (1991).
##Exposure age assumes zero erosion.
***Samples referenced to Z92-0222 standard, which is equivalent to the KNSTD standard.

in Figure 3; field investigation by the authors of this study suggests that this fault dies out toward the southwest.

In addition, these profiles reveal variations in Holocene fault scarp morphologies. Profile 2 displays a 2.43 m vertical offset with a possible two-event morphology, including apparent vertical offsets of 0.78 m and 1.65 m; profile 3 displays a single-event morphology with a 2.05 m vertical offset; and profile 4 displays 4.99 m total offset with a possible two-event morphology, with apparent vertical offsets of 2.99 m and 2.00 m (Figs. 5 and 6). Figure 6B clearly shows the significant variation in scarp morphology, with single- (profile from Bormann et al., 2012) and possible two-event (profile 4, this study) scarp morphologies present within 50 m, measured along strike. As with the older escarpment, the variation in total displacement and the possible number of events recorded by Holocene scarp exposures is at least in part related to the thickness of alluvial cover that has obscured the lower segments of the scarp, with no evidence of a Holocene scarp present along profile 1 because of the actively aggrading alluvial cone with an apex to the southwest of profile 1 (Fig. 3).

Importantly, Holocene scarps that cut young alluvial deposits to the southeast of the Penrod Canyon pediment display en echelon geometries and exhibit both one- and possibly two-event scarp morphologies in close proximity (Fig. 7). These geometries suggest the likelihood of displacement transfer between small-scale propagating segments, adding yet another factor that likely affected the morphologies of Holocene scarps adjacent to the abandoned Penrod Canyon pediment. For instance, for a single earthquake in which upward and along-strike propagating slip breaks the surface of alluvial fans along the range front, it is possible that these slip fronts propagate toward each other but are slightly offset, resulting in apparent two-event morphologies at one location and single-event morphologies at another adjacent location that were created in the same event (see one- versus possible two-event scarps in Fig. 7).

Cosmogenic Nuclide Exposure Age Dating

Bormann et al. (2012) dated samples from the two largest boulders on the Penrod Canyon alluvial surface, C1 and C2 (boulder C2 was also labeled CWL1 in that publication). Two samples from the tallest boulder, C2, yielded ^{10}Be ages with 1σ uncertainties of 84.5 ± 1.7 ka and 111.9 ± 2.7 ka and ^{26}Al ages with 1σ uncertainties of 108.8 ± 4.8 ka and 118.1 ± 6.4 ka (Table 1). A sample from boulder C1, ~0.5 m shorter than boulder C2, yielded a ^{10}Be age with

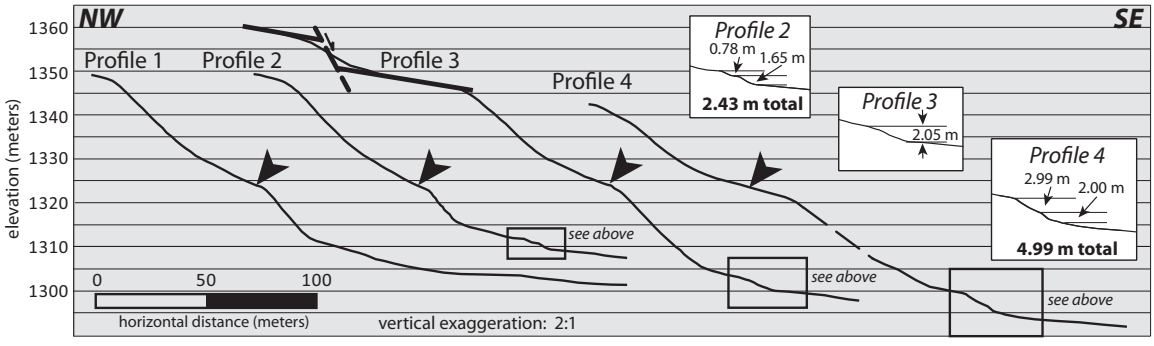

Figure 5. Topographic profiles across the Penrod Canyon escarpment with insets of Holocene fault scarps for profiles 2, 3, and 4 and position of the eroded late Pleistocene wave-cut bench shown (black, bold arrowheads; Qflp in Fig. 3). Profiles 1 through 4 display vertical displacements of the upper alluvial surface and the active alluvial surface of ~45 m, 40 m, 47 m, and 48 m, respectively. The fault identified by House and Adams (2009) is evident in profile 3 (inferred position and orientation indicated), and the profile shown indicates a vertical offset associated with that fault of ~7.0 m. Inset Holocene scarp profiles suggest significant variations in the morphologies and apparent offsets at different profile positions.

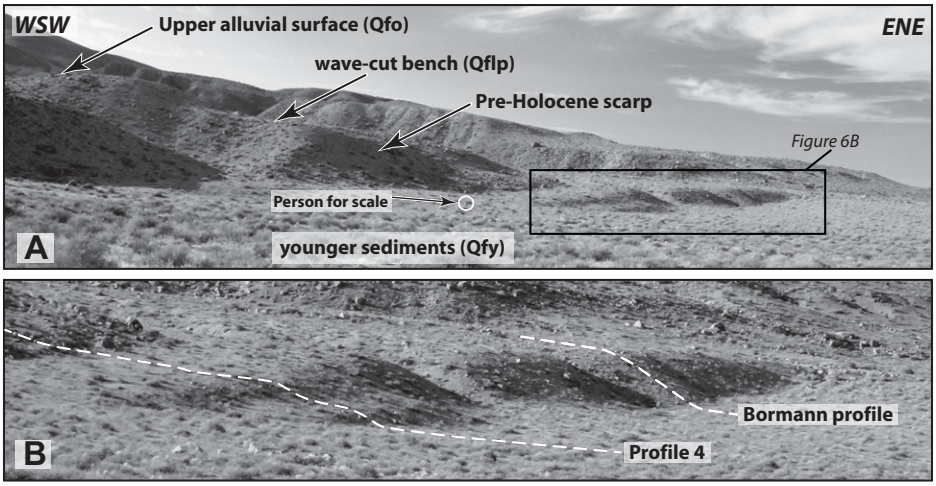

Figure 6. Field photographs of pre-Holocene and Holocene fault scarp exposures, looking NNW (photo taken from the approximate position of the ESE end of the seismic-refraction survey, shown as the "S" symbol in Fig. 3). (A) Pre-Holocene scarp, late Pleistocene wave-cut bench with fluvial and lacustrine deposits (Qflp), and upper surface of the abandoned Penrod Canyon pediment (Qfo) (Fig. 3). The box indicates the location of part B. (B) Holocene scarps, with evident variation in scarp morphology. Vertical offset across the Holocene scarp at the Bormann et al. (2012) location is ~7 m, with a single-event morphology, while just 50 m to the SW, profile 4 reveals a clear two-event morphology with a total vertical offset of ~5 m (Fig. 5). Alluvial deposition has apparently obscured the scarp to the northeast and southwest.

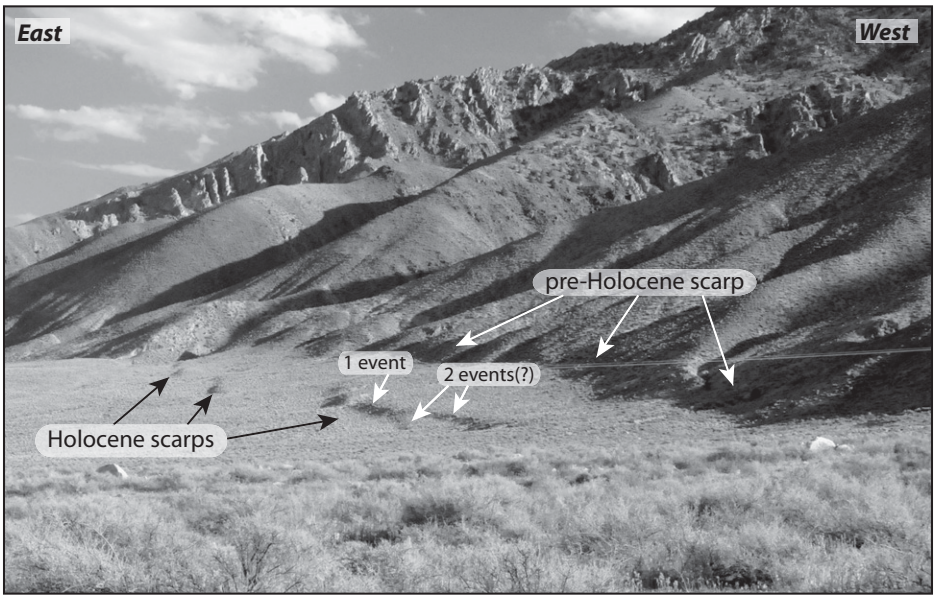

Figure 7. View of both pre-Holocene and Holocene scarps south of Penrod Canyon (photo taken from approximate position of the ESE end of the seismic-refraction survey, shown as the "S" symbol in Fig. 3). Note the discontinuous nature of the exposures and the left-stepping, en echelon distribution of Holocene scarps. These scarps are ~50 m to the ENE of the older, pre-Holocene scarp preserved in Mesozoic bedrock. Similar to the scarp morphologies adjacent to the Penrod Canyon pediment (Figs. 3 and 6), the scarps closest to the viewer reveal variation in morphologies. It appears that the scarp closest to the viewer has accommodated displacement along two faults (two events?), which appear to be splays that merge with the fault to the south, which displays a single-event morphology. See text for discussion. Scarps in photo are similar in scale to the Holocene scarps shown in Figure 6B.

1σ uncertainty of 75.7 ± 1.7 ka, and a ^{26}Al age and uncertainty of 89.6 ± 4.6 ka (Table 1). As discussed in Bormann et al. (2012), the ^{10}Be ages for sample C1 and for one of the two ^{10}Be ages from sample C2 were above the accepted ^{26}Al/^{10}Be production ratio of 6.75 (Table 1; Nishiizumi et al., 2007), so these ^{10}Be ages were not included in age calculations. Bormann et al. (2012) determined preferred exposure ages for boulders C1 and C2 at 89.6 ± 4.6 ka (^{26}Al age) and 112.9 ± 12.5 ka (three sample age grouping, using the two ^{26}Al ages and one ^{10}Be age), respectively. See Bormann et al. (2012) for further discussion.

Samples from boulders C3, C4, and C5, all shorter than boulders C1 and C2 (Table 1), yield ^{10}Be exposure ages with 1σ uncertainties of 73.3 ± 1.3 ka, 69.8 ± 1.8 ka, and 57.2 ± 1.4 ka, respectively, and ^{26}Al ages of 82.2 ± 7.0 ka, 76.3 ± 6.4 ka, and 62.5 ± 6.6 ka, respectively (Table 1). Exposure ages for both methods are concordant within 1σ for samples C3 and C4, while sample C5 is concordant within 2σ for ^{26}Al but not ^{10}Be (Fig. 8A). Based on both new and published data, it is clear that sample exposure ages for boulders C1, C3, C4, and C5 are significantly younger than boulder C2 (Fig. 8A).

We plotted sample exposure ages from the upper alluvial surface of the Penrod Canyon pediment on probability density function (PDF) diagrams (Figs. 8A–8C). Each sample is shown as a Gaussian distribution with a mean and standard deviation from the age and 1σ analytical error. This permits us to test whether analytical uncertainty (Guilderson et al., 2003) is sufficient to explain the distribution of data. On the same diagram, we include the cumulative PDF for all boulders on the alluvial surface, summing the individual PDFs for all boulders in order to identify groups and outliers among the boulder ages.

As discussed in Bormann et al. (2012), it is common to see significant spread in boulder exposure age estimates for depositional features such as the upper surfaces of alluvial fans (e.g., Hoeft and Frankel, 2010; Heyman et al., 2011; Rood et al., 2011). Since weathering, exhumation, and shielding of surfaces by sediment or snow will lead to ages that are younger than the true age of the landform (e.g., Heyman et al., 2011; Owen et al., 2011), we assume that the ages for the boulders exposed on the Penrod Canyon pediment (Fig. 8) are the minimum exposure ages for each sample. As expected, the summative PDFs for both ^{10}Be and ^{26}Al ages display significant spread in boulder ages (Fig. 8). Since the source area for the Penrod Canyon alluvial surface is small, limited to a single primary drainage with no sedimentary deposits exposed within that drainage, it is

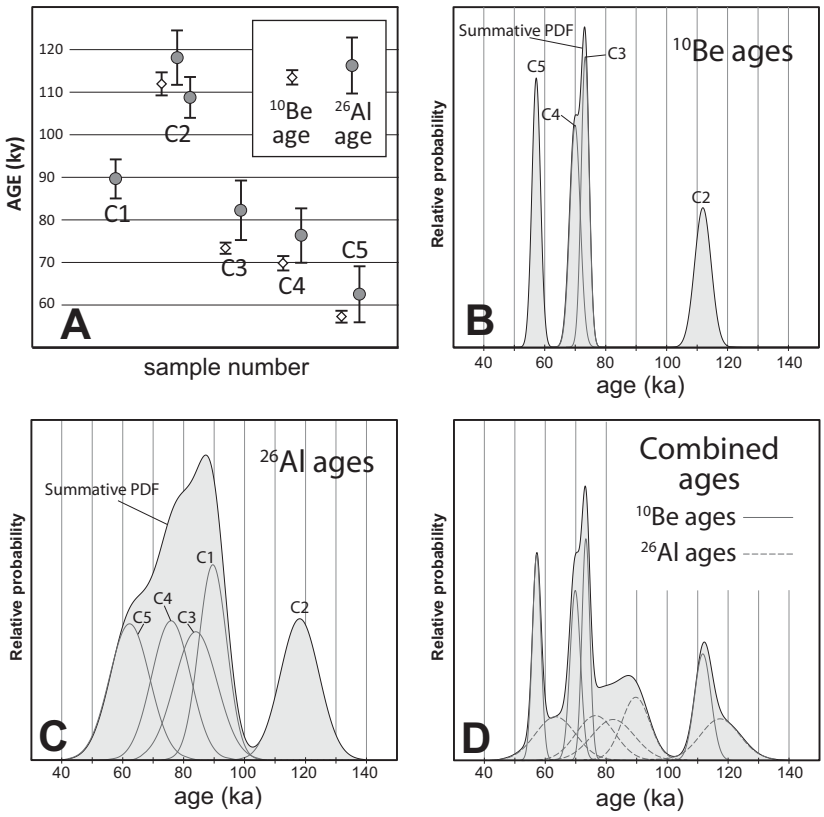

Figure 8. ^{10}Be and ^{26}Al exposure ages of five boulders on abandoned Penrod Canyon pediment surface. (A) Summary of age data for all samples. Open diamonds represent ^{10}Be ages, and filled circles represent ^{26}Al ages. Error bars shown are 1σ. Age data from samples C1 and C2 are from Bormann et al. (2012). (B–D) ^{10}Be and ^{26}Al exposure age probability density function (PDF) diagrams. Shaded area on each diagram represents the summation PDF for all samples. (B) ^{10}Be exposure ages for samples C2, C3, C4, and C5. (C) ^{26}Al exposure ages for samples C1, C2, C3, C4, and C5. (D) Combined ^{10}Be and ^{26}Al exposure ages for samples C1, C2, C3, C4, and C5. See text for discussion.

unlikely that any of these samples experienced prolonged exposure as part of older sedimentary sequences (inheritance). In addition, several studies have indicated that the height of the top of a sampled boulder correlates with exposure age on a given alluvial surface, with taller boulders recording older ages (e.g., Hanks et al., 2001; Putkonen and Swanson, 2003; Garvin et al., 2005; Blard et al., 2007; Behr et al., 2010). Workers have attributed this correlation to post-depositional, erosional surface lowering, where the taller clasts on the present-day surface were exposed to cosmogenic radiation earlier than shorter clasts (e.g., Hanks et al., 2001; Putkonen and Swanson, 2003; Garvin et al., 2005; Blard et al., 2007; Behr et al., 2010). Thus, the tallest boulders exposed on an alluvial surface are expected to provide more accurate estimates of a geomorphic feature's age.

Therefore, we assume that the largest, tallest boulder (C2) preserves the most likely depositional age of 112.9 ± 12.5 ka for the alluvial surface, while the younger sample ages for smaller, shorter boulders reflect lower exposure times to cosmic radiation (due to the surface lowering) and possible small, gravity-driven rotations, which would also reduce sample exposure age. This hypothesis is consistent with both the younger sample ages for the shorter boulders as well as the minor, but observable, erosion associated with the small drainage systems that have dissected the pre-Holocene escarpment (Fig. 3). Based on this age and the vertical offset between Qfo and the present-day Qfy surface, we could estimate a minimum rate of vertical displacement along the fault system (consistent with Bormann et al., 2012), but geophysical data provide information about the same Qfo surface in the buried hanging wall, thus permitting us opportunity to more rigorously constrain the time-averaged rate of vertical displacement at the 10^5 yr time scale.

Seismic Refraction

The seismic velocity model shows a clear break from velocities less than 1000 m/s to very high apparent velocities, suggesting a high-velocity layer dipping eastward away from the surface scarp. Downdip shots do not show apparent breaks in velocity, preventing us from utilizing discrete layer analysis techniques, so we chose to interpret the data using a tomographic approach.

We performed a series of tomographic inversions using Geogiga's DWTomo software, which employs grid ray tracing and regularized inversion. A variety of starting models, including constant velocities, vertical velocity gradients, horizontal layers, and dipping layers, converged to similar results. The best-fit tomographic model shown in Figure 9 was inverted from a vertical gradient starting model. Root mean square (RMS) residuals between picks and calculated traveltimes were less than 2.5 ms. The approximate depth resolution for this model is ±5 m. Figure 9A is the best-fit tomographic model with raypaths shown for reference, and Figure 9B is the best-fit model with our interpretation of subsurface geology.

The model implies shallow unconsolidated sediment with velocities in the 500–900 m/s range extending laterally across the survey area, extending to the southeast from profile 2 (Fig. 5). At the northwest end of the line, adjacent to the scarp, these sediments extend to depths of less than 5 m and deepen to ~40 m at the southeast end of the line away from the scarp (deep blues and purples in Fig. 9). Beneath these unconsolidated sediments, there is a wedge-shaped body with velocities in the 1000–1400 m/s range (light blues and greens in Fig. 9), thickening northwestward. We suggest that this deeper, higher-velocity material is most likely proximal post-Qfo sediments (Fig. 9B). The geometry at the northwest end of the survey is consistent with buried colluvium or debris flows adjacent to the scarp, which would be expected with deposits adjacent to an active normal fault scarp. Beneath this material, velocities increase into the 1500–2500 m/s range (yellows and oranges in Fig. 9), suggesting a granitic bedrock surface dipping from ~50 m depth at the northwest end of the line to ~55 m in the southeast. The length of the survey line and depth of ray penetration do not permit a delineation of velocities below ~70 m.

Based on the best-fit model's velocity gradient above the highest velocities, we hypothesize that the granitic bedrock is overlain by granitic regolith and Qfo deposits (Fig. 9B), similar to what we documented in the exposed footwall (Fig. 3). These results indicate that the bedrock

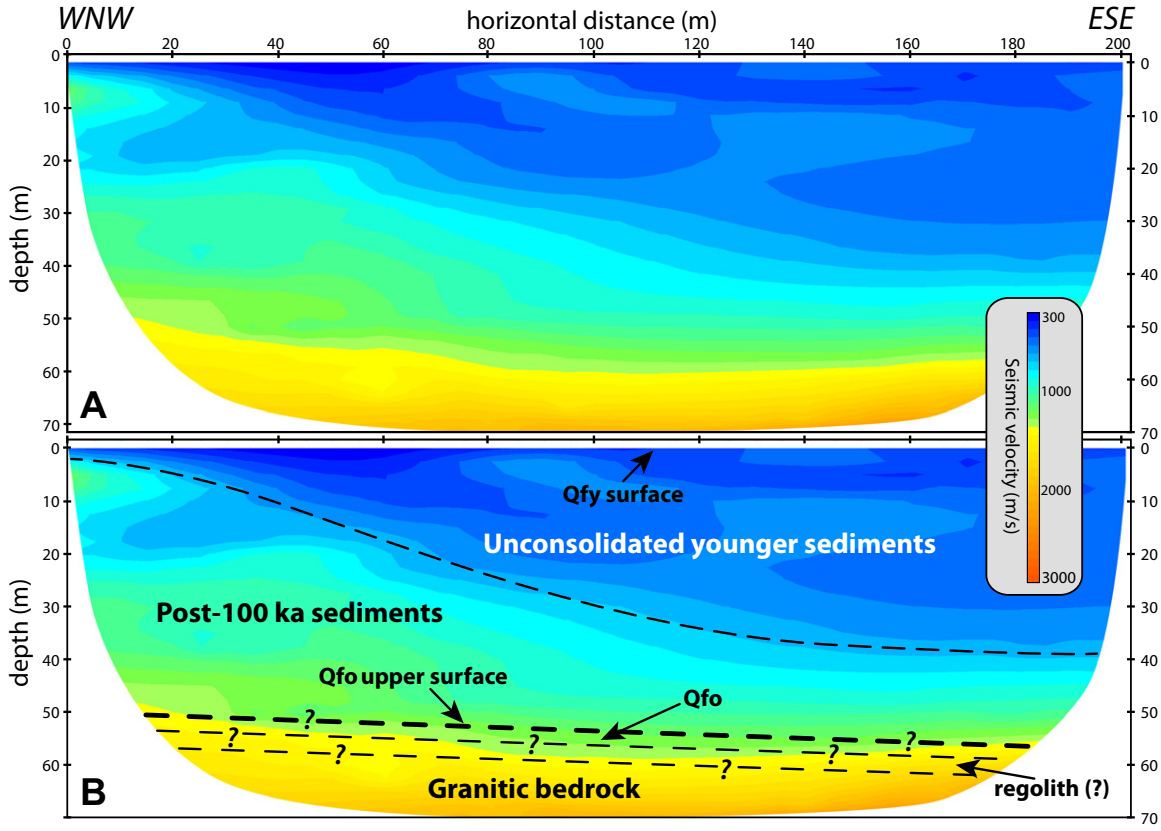

Figure 9. Shallow seismic tomography results. (A) Best-fit seismic tomographic model without geologic interpretation. Colors indicate calculated velocities beneath seismic survey line shown in Figure 3. All depths shown are measured relative to the surface of Qfy (younger Quaternary fanglomerates), which slopes at approximate 2.5° to the southeast. We interpret the approximate position of map unit Qfo (older Quaternary fanglomerates) based on the model velocities shown here. (B) Best-fit tomographic model with interpretation of subsurface geology. Due to decreasing resolution with increasing depth, the precise positions of boundaries between the units shown in B are not well constrained by seismic data (approximate depth resolution is ±5 m).

pediment surface presently lies at 50 ± 5 m depth in the hanging wall adjacent to the fault scarp, and when corrected to account for the 2.5° dip of the upper Qfy surface, the dip of the Qfo-Mu surface in the subsurface hanging wall is consistent with the estimated 4.5° dip of the Qfo-Mu contact documented in the footwall.

Gravity

The corrected survey data from the free-air reduction reveal values that range from 3221 mGal on the WNW end of the survey to 3208 mGal at the ESE end of the survey ("observed" data in Fig. 10A). From WNW to ESE, these data display a gently concave-down profile until ~500 m, where the gravity profile becomes concave-up. Observed gravity values to the ESE of the 600 m mark become relatively linear, with a gentle decrease to the end of the survey (Fig. 10A). We used an iterative approach to forward modeling in an attempt to best reproduce this anomaly. In all of our modeling, we constrained density values to 2.65–2.67 g cm^{-3} for the Mesozoic bedrock and 2.00 g cm^{-3} for the sedimentary units.

Our initial model, which consisted of a vertical contact between the Mesozoic and Quaternary bodies, produced a gravity anomaly that fit the far-field gravity differences on the east and west ends of our line, but the transition between high and low gravity values was far too steep. By reducing the dip of the fault to 75° and adding a thin wedge of sedimentary cover (colluvium from the upper surface of the footwall pediment), we developed a two-body system (Fig. 10B) that fit the corrected gravity profile well ("model" values in Fig. 10A). Although other two-body models also produced values similar to the model chosen, fault dip values between 55° and 75° were the only dips that resulted in values similar to the chosen best-fit model. While the chosen model is relatively simple in the number of bodies used, gravity interpretations from a single line are not unique. More complicated subsurface geometries and densities are not warranted (e.g., Grosfils et al., 2003).

The gravity data support a relatively simple system, with one dominant, high-angle fault located at the approximate position of the larger, pre-Holocene fault scarp. The smooth, low-gradient gravity data to the WNW of the pre-Holocene scarp (Fig. 10) imply that no significant fault system truncates the abandoned Penrod Canyon pediment surface in the footwall of the system. Although House and Adams (2009) identified a normal fault WNW of and subparallel to the range-front fault (Fig. 3), it appears that displacement (7.0 m at profile 3; Fig. 5) rapidly decreases along strike to the SSW of profile 3, such that any remaining displacement cannot be detected by gravity data collected ~50 m to the SSW (Figs. 3 and 10). Although the discontinuous Holocene scarp system documented by other workers (e.g.,

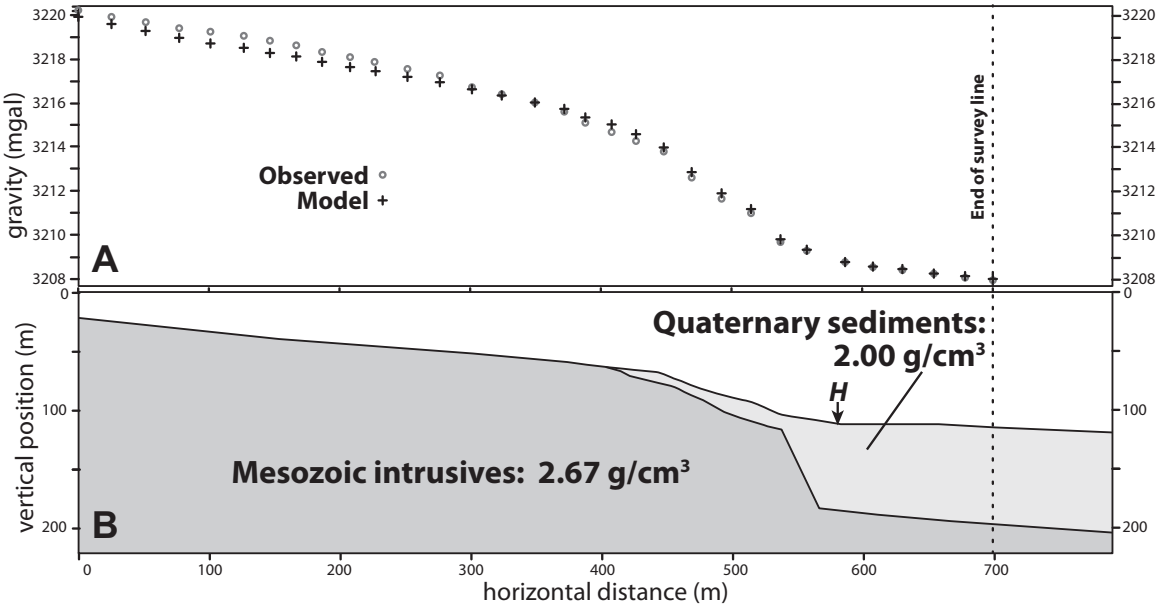

Figure 10. Gravity data and model results from the Penrod Canyon fault. (A) Observed gravity data (gray circles, in mGal), plotted with best-fit model data (black crosses). (B) Best-fit body model, assuming approximate densities of 2.67 g/cm³ and 2.00 g/cm³ for Mesozoic intrusive units and Quaternary sediments, respectively. Holocene scarp position (H in B) is outboard of both the topographically defined pre-Quaternary fault scarp and the gravity-defined position of the dominant fault plane.

Demsey, 1987; Wesnousky, 2005; Bormann et al., 2012) is located ~20–30 m to the ESE of the older scarp, gravity data do not suggest significant displacement at that location (Fig. 10). Instead, we suggest that the Holocene scarps define a fault splay that soles into the older and much larger-offset normal fault at this location. Importantly, there are no significant inflections in the monotonously decreasing gravity values to the ESE of the fault scarps, consistent with an intact, gently dipping bedrock surface, with a dip that is very similar to the ESE dip of the exposed pediment surface in the footwall (~4.5°).

The most significant deviations between observed and model data occur between the 0 m and 250 m mark, which coincides with the WNW end of the gravity survey (Figs. 3). The Mu-Qfo contact on the margins of the dissected pediment is not well exposed, thus preventing direct observation of relief along the contact. However, the upper surface of the pediment, while not part of the major drainage systems to the northeast and southwest, does reveal minor erosion associated with small drainage systems, which would, in effect, reduce the sediment thickness at different locations along the survey line (Fig. 3). Based on these observations, we suggest that the deviation observed is likely related to a combination of variations in sediment thickness and minor relief in the underlying Mu-Qfo contact.

Faceted-Spur Analysis

Our faceted-spur analysis of the Wassuk Range normal fault indicates significant variation in facet height and therefore long-term (>1 m.y.) vertical throw rate (Petit et al., 2009a, 2009b) along the fault system (Table 2; Fig. 11A). The seven identified facets display an average height of 672 m with a standard deviation of 154 m. If we calculate the long-term slip rate based on this average and standard deviation, we obtain a slip rate of 0.87 ± 0.20 mm/yr (Table 2). However, we suggest that documented differences in slip rate vary spatially, based on facet position along the Wassuk Range fault system. When we use the linear relationship between facet height (in m) and vertical throw rate (in mm/yr) established by Petit et al. (2009b), it becomes clear that the lowest slip rate values are derived from facets in the northern Wassuk Range (based on facets N-1 and N-2; Table 2; Figs. 2 and 11A), and the highest values are located in the southern Wassuk Range, near Rose Creek and Mount Grant (based on facets S-4 and S-5; Table 2; Figs. 2 and 11A). Differences in facet heights suggest a long-term slip rate as low as 0.60 ± 0.20 mm/yr to the north of Penrod Canyon and rates as high as 1.13 ± 0.20 mm/yr near Mount Grant and Rose Creek (Fig. 2; Table 2). Using the heights of faceted spurs S-1, S-2, and S-3,

TABLE 2. FACETED-SPUR DATA AND ANALYSIS

Facet name	Latitude (°N)	Longitude (°W)	Facet top (m)	Facet base (m)	Facet angle (°)	S_v (mm/yr)*	Crest elev.† (m)
N1	38°54′20″	118°49′19″	1796 ± 10	1336 ± 10	18.9 ± 0.7	0.60 ± 0.20	2312
N2	38°53′28″	118°48′45″	1830 ± 10	1300 ± 10	17.8 ± 0.5	0.69 ± 0.20	2447
S1	38°48′17″	118°47′15″	2063 ± 10	1334 ± 10	21.3 ± 0.5	0.95 ± 0.20	2750
S2	38°44′42″	118°47′32″	1923 ± 10	1269 ± 10	18.3 ± 0.4	0.85 ± 0.20	2542
S3	38°40′17″	118°46′26″	1824 ± 10	1210 ± 10	29.6 ± 0.9	0.80 ± 0.20	2339
S4	38°34′59″	118°43′40″	2386 ± 10	1513 ± 10	28.9 ± 0.6	1.13 ± 0.20	3442
S5	38°33′58″	118°42′46″	2255 ± 10	1410 ± 10	23.5 ± 0.5	1.10 ± 0.20	3442
				Average	22.6	0.87	2753
				SD§	4.9	0.20	492
				Range	17.8–29.6	0.60–1.13	2312–3442

*S_v is the vertical throw rate: error based on spread in calibration data shown on fig. 3A from Petit et al. (2009b) (see Fig. 11).
†Crest elevation is the elevation of the range crest where the spur meets the range crest.
§SD—standard deviation.

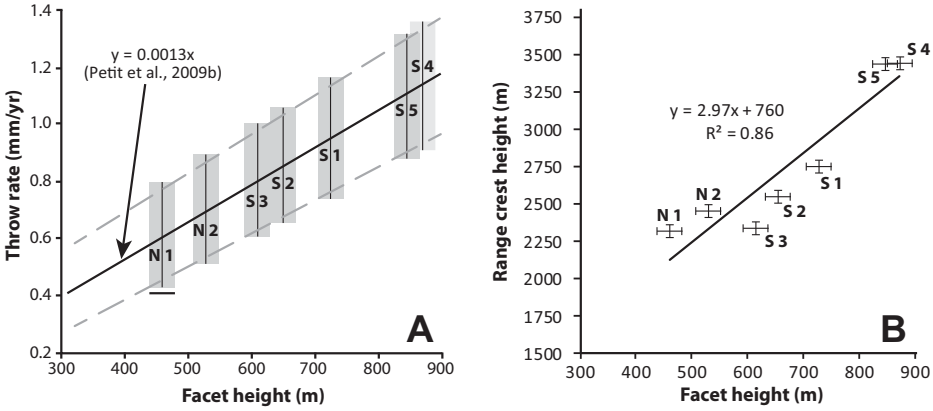

Figure 11. Facet-analysis data from the Wassuk Range normal fault system. (A) Vertical throw rate as a function of facet height, based on the results of Petit et al. (2009a, 2009b). Black line is the best-fit line from Petit et al. (2009b) that relates facet heights to throw rates calculated in the literature for the fault systems analyzed by Petit et al. (2009a, 2009b). The dashed gray lines represent the upper and lower bounds of the data displayed in Figure 3B of Petit et al. (2009b). The width of each gray box indicates the approximated error in facet height for each Wassuk Range facet, the black line represents the documented facet height value, and the height of the boxes is the approximate error that we have assigned based on the spread in data used by Petit et al. (2009b). (B) Individual facet heights plotted against range crest heights (measured adjacent to each faceted spur). These data support a strong (R^2 = 0.86), positive linear relationship between these measurements.

we calculated vertical displacement rate values of 0.95 ± 0.20 mm/yr, 0.85 ± 0.20 mm/yr, and 0.80 ± 0.20 mm/yr, respectively, which are intermediate between the northernmost and southernmost slip values (Table 2; Fig. 2).

Interestingly, we document a strong, positive linear relationship between facet height and range-crest height in the Wassuk Range, with a relatively high R^2 value of 0.86 (Fig. 11B). Because facet height can be directly related to long-term slip rate along major normal fault systems (Petit et al., 2009a, 2009b), we suggest that relative topographic relief of mountain ranges in the footwalls of major normal fault systems can be used as qualitative proxies for strike-parallel variations in vertical displacement rate.

DISCUSSION

Range-Bounding Fault Evolution at Penrod Canyon

Based on geologic, cosmonuclide exposure age, and geophysical data, we present a model of the active Wassuk Range normal fault system at Penrod Canyon (Fig. 12). The well-preserved, abandoned Penrod Canyon pediment is cut by a significant normal fault at a right step in the Wassuk Range fault system (Figs. 2 and 3). We used the contact between the abandoned mantle of alluvium and the suballuvial bedrock pediment as a marker to estimate the total vertical displacement that has taken place since the time that the upper alluvial surfaced was active. These data support a total vertical displacement value of 90 ± 7 m, based on sum of footwall relief (40 ± 2 m) and burial of the hanging wall by alluvium (50 ± 5 m). We also suggest that there is a single, high-angle fault system that has accommodated most slip, with younger Holocene faults likely soling into the larger, high-angle structure (Fig. 12).

We also posit that the eastward-thickening wedge of low-velocity post–100 ka material evident on our seismic-refraction tomographic model (Fig. 9) is composed of both small-scale debris-flow deposits and colluvium eroded from the scarp itself (Fig. 12). This would be consistent with the expected distribution of sediments adjacent to an active normal fault system, with finer, more thinly bedded sediments at greater distances from the scarp. We base our interpretation of the subcolluvial bedrock scarp shape, with its two concave-up segments (Fig. 12), on gravity data (Fig. 10), the distribution of lacustrine platform deposits (Qflp; Fig. 3), and the well-established wave-cut cliff and platform structure associated with lake-level highstands at locations throughout the Basin and Range (e.g., Wesnousky, 2005; Jewell and Bruhn, 2013). We suggest that later, wedge-shaped colluvial deposition covered the bedrock shapes, resulting in the observed present-day scarp profiles (Figs. 5 and 12). Importantly, gravity data (Fig. 10) support the presence of a thin layer of sediments on

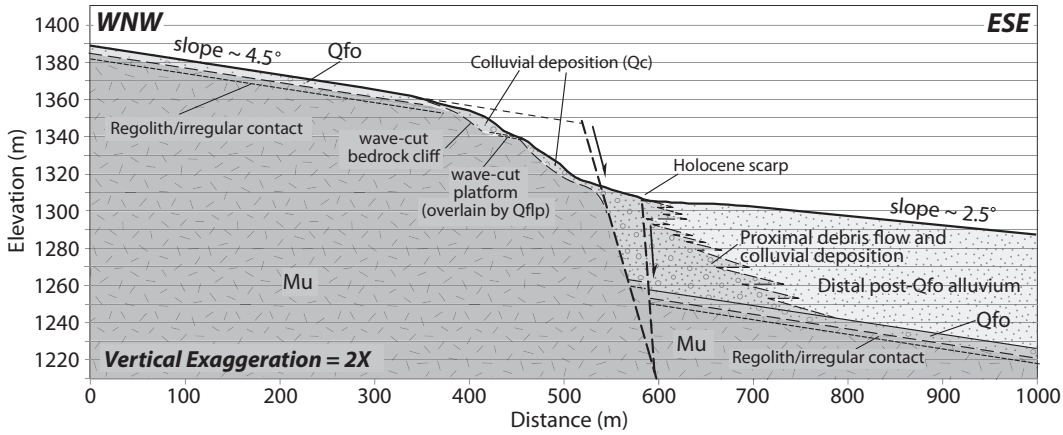

Figure 12. Cross-sectional interpretation of the Wassuk Range normal fault system based on geologic and geophysical data. We suggest that the fault system that has created Holocene scarps along much of the Wassuk Range soles into the fault system that has created topographic relief and pre-Holocene scarps along the range front. Field and geophysical data support the likelihood that proximal alluvial deposits are composed of debris-flow deposits and colluvium, with rapidly decreasing clast size with distance from the degraded pre-Holocene scarp. This interpretation suggests a total displacement of ~90 m since active Qfo deposition, resulting in a time-averaged slip rate of 0.82 ± 0.16 mm/yr at the 10^5 yr time scale. Map units defined in Figure 3.

the eroded footwall proximal to the fault trace. Based on these interpretations of subsurface structure, resulting in a total vertical displacement across the fault system of 90 ± 7 m, and our interpretation that the oldest boulder exposure age of 112.9 ± 12.5 ka is an accurate date for the minimum age of the upper alluvial surface (Qfo), we derive a minimum vertical displacement rate of ~0.82 ± 0.16 mm/yr since ca. 113 ka.

In addition, we suggest that formation and preservation of the Penrod Canyon pediment occurred because of unusual local structural geometry, with relative geomorphic stability created by a small embayment in the mountain front (e.g., Dohrenwend, 1982; Dohrenwend and Parsons, 1994). The older Miocene fault system that cuts the Wassuk Range at a high angle to the mountain front (Fig. 2) has likely affected the post-Miocene evolution of the east-dipping range-front fault system, resulting in the right step along the present-day mountain front. Without this structural geometry, it is unlikely that the bedrock pediment would have been preserved. The pediment's abandonment and subsequent preservation might also be related to a stream-capture event at the approximate time of abandonment, with the Reese River Canyon to the north (Fig. 2) capturing most flow from the Penrod Canyon drainage system, thus preserving the pediment (S. Wesnousky, 2014, personal commun.).

Our analysis of the spatial relationships and morphologies of the Holocene scarps near the primary fault trace reveals the complex nature of the development of these young systems. These scarps commonly display en echelon distributions (Fig. 7), with apparent vertical displacements dying out toward the end of each segment as displacement is likely transferred to another segment. In some cases, it is possible that a single scarp may have accommodated two earthquake events, while in other cases, what may be interpreted as a scarp with evidence for two events may instead be a location where two upward- and laterally propagating segments may have interacted to form a morphology consistent what might be considered a possible two-event scarp (Figs. 6B and 7). Based on these observations and previous studies (e.g., Bormann et al., 2012; Wesnousky et al., 2012), we suggest that care be taken in interpreting the surface morphology of young fault scarp systems.

Long-Term Vertical Displacement Rates from Faceted-Spur Analysis

Our faceted-spur analysis reveals spatial variations in long-term throw rates along the range-front fault system (Table 2; Figs. 2 and 11), with the lowest slip rates along the northern portions of the fault system and the highest slip rates along the southern section of the fault, near Mount Grant. The two faceted fault spurs closest to the Penrod Canyon pediment, N-2 and S-1, suggest long-term (>1 m.y.) vertical displacement rates between 0.69 ± 0.20 mm/yr and 0.95 ± 0.20 mm/yr, respectively (Table 2; Fig. 11). However, it appears that the pre-Quaternary fault system that runs through Penrod Canyon and Reese River Canyon, immediately to the north (Fig. 2), has likely accommodated different vertical displacement rates along sections of the Wassuk fault to the south and north of this structure. This hypothesis is supported by the significant decrease in average range crest height from ~2620 m to the south of Penrod Canyon to 2310 m to the north, based on profiles measured along ~10 km of the range-crest drainage divide (Surpless and Bentz, 2011). Thus, we use the vertical displacement rate from facet S1, 0.95 ± 0.20 mm/yr, for the section of the Wassuk Range normal fault system at the latitude of the Penrod Canyon pediment.

Our data suggest that variations in range crest elevations can be tied to along-strike changes in slip rate, with the lowest crest elevations and vertical displacement rates in the north and the highest range crest elevations and vertical displacement rates in the south, near Mount Grant, the highest peak in the Wassuk Range (Fig. 2; Table 2). Our findings are supported by the work of Gorinski et al. (2013), who suggested that the fault near Mount Grant has slipped at a higher vertical displacement rate than the Wassuk fault further north. Importantly, these results are also consistent with the findings of Kirby et al. (2008), who suggested that topographic relief in areas of active deformation can be used to qualitatively determine variations in rock uplift rate.

Temporal Variation of Vertical Displacement Rates

When combined with previous studies of vertical displacement rate along the Wassuk Range fault system, our data support a relatively constant long-term rate since ca. 4 Ma (Table 3; Fig. 13A). At most time scales, there is some concordance between rates of slip; we prefer a vertical displacement rate that has remained fairly constant at 0.75–1.0 mm/yr from ca. 4 Ma to the present, a range in slip rates that overlaps with slip rate estimates at nearly all time scales (Fig. 13A). Interestingly, this would suggest that most of the present-day relief of the Wassuk Range has been produced since ca. 4 Ma, consistent with the results of structural reconstructions and thermochronologic data that suggest a renewed pulse of normal fault motion starting at that time (Stockli et al., 2002; Surpless et al., 2002; Surpless, 2011). Importantly, we suggest that our new slip rate estimate for the 10^5 yr time scale spans sufficient time that the effects of earthquake clustering, on the ~10^4 yr time scale (e.g., Friedrich et al., 2003), are negligible in time-averaged displacement rate calculations (Fig. 13B). Vertical displacement rates at the ~10^4–10^3 yr time scale, however, are more variable (Table 3; Fig. 13A) and require explanation in the context of long-term rates.

There is significant mismatch for the vertical displacement rates estimated by Bormann et al. (2012) and Dong et al. (2014) at similar time scales (0.7 ± 0.1 mm/yr since ca. 10 ka and 1.0–1.5 mm/yr since 20 ka, respectively; Table 3; Fig. 13A). There are several possible explanations for these mismatches in slip rate at the 10^4–10^3 yr time scale. It is possible that additional vertical displacement is being accommodated on faults outboard of the Rose Creek trench location where Bormann et al. (2012)

TABLE 3. WASSUK RANGE VERTICAL DISPLACEMENT RATES

Time period	Reference	Method	Vertical displacement rate (mm/yr)
Post–4 Ma	Stockli et al. (2002)	Low-temperature thermochronologic modeling	0.5–0.75
>1 Ma to present	This study	Fault scarp facet height analysis	0.95 ± 0.20
Post–100 ka	This study	Geologic, geophysical, and cosmogenic exposure age data	0.82 ± 0.16
Post–20 ka	Dong et al. (2014)	High-resolution seismic CHIRP* profiles	1.0–1.5
Holocene	Bormann et al. (2012)	Trench excavation	0.7 ± 0.1
Modern	Wesnousky et al. (2012)	Geodetic analysis† (central Wassuk Range)	0.4–1.2
Modern	Wesnousky et al. (2012)	Geodetic analysis† (northern Wassuk Range)	0.9–1.7

*CHIRP—compressed high-intensity radar pulse.

†Reported as range in fault-perpendicular horizontal extension rate (based on 0.4–0.7 mm/yr for the central Wassuk Range and 0.9–1.0 mm/yr for northern Wassuk Range). Values in table are equal to the horizontal extension rate multiplied by the tangent of the fault dip (vertical displacement rate = horizontal extension rate × tan θ). Based on previous geologic and geophysical studies and this study, we assume that fault dip is likely between 45° and 60°.

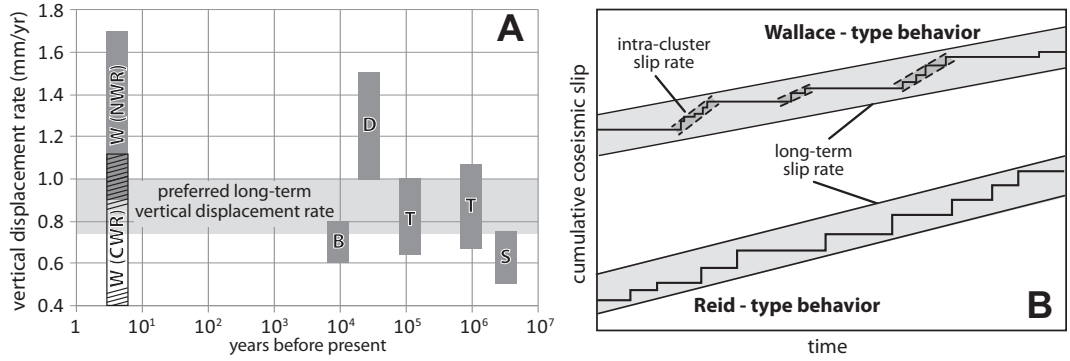

Figure 13. Temporal estimates of time-averaged vertical displacement rates for the Wassuk Range fault and theoretical Wallace-type and Reid-type fault behaviors. (A) Shaded light-gray region displays our preferred long-term vertical slip rate of 0.75–1.0 mm/yr for the Wassuk Range fault. Abbreviations: W (CWR)—Wesnousky et al. (2012) estimate for central Wassuk Range (diagonal striped region); W (NWR)—Wesnousky et al. (2012) estimate for northern Wassuk Range (dark-gray region); B—Bormann et al. (2012); D—Dong et al. (2014); T—this study; S—Stockli et al. (2002). See text for discussion. (B) Theoretical Wallace-type (e.g., Wallace, 1987) and slip-predictive Reid-type (e.g., Reid, 1910; Shimazaki and Nakata, 1980) behaviors. Although the long-term slip rates for both behaviors would be similar, in Wallace-type behavior, most coseismic slip is released during short periods of earthquake clusters, with significantly longer periods of quiescence. In Reid-type behavior, coseismic slip is released over time without significant clusters.

made their observations (which would increase the calculated vertical displacement value since ca. 10 ka), with unrecognized faulting offshore or obscured by recessional shorelines of ancestral Lake Lahontan. However, the geomorphic expression of faulting along the range front at that location does not indicate significant slip outboard of the apex of the Rose Creek alluvial fan. It is also worth noting that we have no way of estimating where the fault near Rose Creek is in the earthquake cycle. For instance, if an earthquake with significant slip were to occur at that locality in the near future, the post–10 ka slip rate value calculated after that event might be similar to the estimate of Dong et al. (2014). Alternatively, the time-averaged slip rate of Dong et al. (2014) might record a "cluster" of earthquakes (e.g., Wallace, 1987; Sieh et al., 1989; Rockwell et al., 2000; Friedrich et al., 2003) between ca. 20 ka and ca. 10 ka, resulting in the higher post–20 ka strain rates documented by Dong et al. (2014). This hypothesis is supported by the findings of Dong et al. (2014), who suggested a possible earthquake cluster between ca. 15.5 ka and 10.5 ka. This is our preferred explanation for the discrepancy between slip rate estimates.

Interestingly, the timing of this hypothesized cluster is similar to the ca. 13 ka Sehoo highstand (Adams and Wesnousky, 1998) of the ancestral Lake Lahontan. At the time of the highstand, the lake covered almost 4° of latitude and 3° of longitude in western Nevada and eastern California, with the Walker Lake basin at the southernmost margin of the ancestral lake (e.g., Adams et al., 1999). Adams and Wesnousky (1998) suggested that the rise of Lake Lahontan lake level prior to this highstand was extraordinarily rapid, an idea supported by numerous other studies (e.g., Benson and Mifflin, 1986; Benson, 1991, 1993; Benson et al., 1995). However, as lake levels rose, not all basins were filled simultaneously due to the different elevations of sills that permitted water to flow into each basin (e.g., Benson and Mifflin, 1986). The lake level of ancestral Walker Lake was initially independent of lake levels in other basins until Lake Lahontan reached a level of 1308 m, which permitted water to flow across the Adrian Valley sill (Fig. 1). Benson and Mifflin (1986) loosely constrained the timing of this event at ca. 14 ka, based on lake-level reconstructions (see fig. 2 *in* Benson and Mifflin, 1986), but it is possible that this level was reached in only decades (e.g., Adams and Wesnousky, 1998, and references therein). We therefore infer that the Walker Lake basin was filled rapidly, perhaps in an abrupt flooding event, immediately prior to the Sehoo highstand at ca. 13 ka.

A flooding event or even a relatively rapid lake-level rise has implications for the triggering of seismicity along the east-dipping Wassuk fault zone. The rapid increase in water depths associated with a lake transgression would have placed an enormous weight of water on the hanging wall of the fault (the Walker Lake basin) and would also have increased the pore-fluid pressure both along and adjacent to the fault. These nontectonic factors would have redistributed stress patterns on the fault in such a manner as to increase shear stress and decrease normal stress on fault planes, thus increasing the likelihood of slip along the fault (e.g., McCalpin and Nelson, 2001; McGarr et al., 2002). This situation is similar to seismicity triggered by manmade reservoirs, where water-level changes of only a few meters a day have been shown to influence the rate of seismicity (e.g., Simpson and Negmatullaev, 1981; Carder, 1970; Roeloffs, 1988; Simpson et al., 1988; McGarr et al., 2002). We therefore suggest that the earthquake cluster reported by Dong et al. (2014) was likely initiated by nontectonic stressors and explains the discrepancy in vertical displacement rates at similar time scales (Bormann et al., 2012; Dong et al., 2014).

The total mass of water present in the Lake Lahontan (and therefore Walker Lake) basin decreased rapidly in the 1000 yr after the Sehoo highstand (~100 m drop in lake level relative to a maximum depth of 170 m; Thompson et al., 1986; Adams and Wesnousky, 1998; Adams et al., 1999). Assuming that Walker Lake was also affected by a similar rate of desiccation, the hanging wall of the Wassuk fault would have experienced a reduced gravitational load, and pore-fluid pressures would similarly have decreased within and adjacent to the fault zone. If we assume that seismicity was triggered as lake levels rose, we must also assume that seismicity may have been suppressed as lake levels fell. It is possible that a portion of the time period documented by Bormann et al. (2012) was affected by a suppression of seismicity, but lake levels across Lake Lahontan have remained low since ca. 10 ka (e.g., Born, 1972; Benson et al., 1992; Briggs et al., 2005; Bills et al., 2007), so although there may have been a reduced slip rate related to lake-level fall between ca. 13 ka and ca. 10 ka, we suggest that those effects should be insignificant in any post–10 ka vertical displacement rate estimate.

The relatively elevated rates of modern deformation (from geodesy) determined by Wesnousky et al. (2012) for the northern Wassuk Range (0.9–1.7 mm/yr; Table 3; Fig. 13) could be explained by the complex sum of postseismic effects from Holocene earthquakes across the region, similar to an explanation offered for the Wasatch fault by Friedrich et al. (2003).

Alternatively, if any significant antithetic simple shear has been accommodated within the hanging wall of the east-dipping Wassuk Range fault during displacement, then these vertical displacement rates are overestimates of the true vertical displacement rate (White et al., 1986; Chang et al., 2006), which might reduce these rates to values consistent with our preferred long-term displacement rate. However, modern strain rates for the northern Wassuk Range are only slightly elevated relative to our long-term slip rate estimate, and vertical displacement rates for the central Wassuk Range (0.4–1.2 mm/yr) significantly overlap with our preferred long-term vertical displacement rate. Thus, we suggest that the relatively constant vertical displacement rate across the Wassuk Range normal fault zone implies that the rate of strain accumulation (recorded by geodetic studies) and the rate of strain release (geologic studies) are similar across the Wassuk Range normal fault zone. In addition, these data suggest that plate-boundary, gravitational and thermal effects on the central Walker Lane, and the Wassuk Range specifically, have remained relatively constant since the late Pliocene.

Although this is consistent with previous comparisons of short- versus long-term time scales across plate boundaries (e.g., DeMets et al., 1994; Sella et al., 2002; Wallace et al., 2004), this contrasts with studies that have documented changes in slip rate over time for smaller fault zones within larger zones of deformation (e.g., Friedrich et al., 2003; Hoeft and Frankel, 2010; Rood et al., 2011). In some cases, mismatches between geodetic (short-term) and geologic (long-term) data have been attributed to postseismic transients (e.g., Friedrich et al., 2003; Pollitz et al., 2008). However, when comparing the behavior of the Wassuk fault to that of the Wasatch normal fault, which has perhaps the best-constrained vertical slip rates in the world (Friedrich et al., 2003), it is clear that changes in slip rate at comparable temporal windows appear significantly different.

Friedrich et al. (2003) documented rates of vertical displacement along the Wasatch fault at 0.5–0.7 mm/yr since 10 Ma, <0.6 mm/yr since 130 ka, and 1.2–2.3 mm/yr since 6 ka (Friedrich et al., 2003), suggesting a significant increase in vertical displacement rate along the fault system at the ~10^3–10^4 yr time scale. Importantly, paleoseismic (trench excavation) studies across the Wasatch fault (McCalpin, 1999; McCalpin and Nelson, 2000) reveal an average Holocene earthquake recurrence interval of ~1.7 k.y. (6 major earthquakes since 10 ka), with pre–10 ka interseismic intervals of 7 k.y. and >10 k.y. These results suggest that conventional earthquake recurrence models ("Reid-type" behavior; e.g., Reid, 1910; Scholz, 1990) cannot be applied to the Wasatch fault system because these slip events would require large, unexplained changes in strain accumulation on the 10 k.y. time scale (Friedrich et al., 2003). Friedrich et al. (2003) posited that Wallace-type behavior (uniform long-term strain accumulation with seismic strain release clustered on the 10^4 yr time scale) best explains the vertical displacement rate history of the Wasatch fault.

McCalpin and Nelson (2001) suggested that the long recurrence intervals of earthquakes along the Wasatch fault between ca. 17 ka and 9 ka coincided with the desiccation of ancestral Lake Bonneville. This desiccation began with a sudden 100 m drop from the Lake Bonneville lake-level highstand at 17.2 ka and continued to the Holocene lowstand of the lake at ca. 13 ka (McCalpin and Nelson, 2001). They proposed that a combination of reduced load on the hanging wall of the fault system and reduced pore-fluid pressures could have suppressed slip along the fault (McCalpin and Nelson, 2001). If a lake regression did indeed inhibit strain release, it is possible that post–10 ka earthquakes along the Wasatch fault have released strain accumulated over a longer period of time, potentially resulting in elevated vertical displacement rates since 10 ka. However, both post–6 ka and modern (geodetic) strain rates across the Wasatch fault are significantly higher than longer-term rates of slip (Friedrich et al., 2003), suggesting that a Wallace-type model remains the best explanation for Wasatch fault behavior.

Although data from the Wassuk fault support an earthquake cluster at the ~10^4 yr time scale, the post–10 ka vertical displacement rate, accommodated by a minimum of three significant earthquakes during this period (Bormann et al., 2012), is very similar to our preferred long-term vertical displacement rate. We suggest that the documented Wassuk fault cluster might be anomalous, triggered by an unusual, nontectonic change in crustal stresses (the rapid transgression of ancestral Lake Lahontan). Thus, we suggest that the Wassuk Range fault system exhibits slip-predictable Reid-type behavior (Fig. 13B), with rates of strain accumulation and release that have remained relatively constant over time.

Therefore, we hypothesize that while the Wasatch fault and the Wassuk fault appear to display Wallace-type behavior, future behavior along the Wassuk fault is perhaps easier to predict. If true, the slip-predictable Reid-type behavior of the Wassuk fault is unusual relative to other major fault systems worldwide. Wallace-type behavior has been documented on segments of the San Andreas fault system (Sieh et al., 1989; Grant and Sieh, 1994), faults associated with the Eastern California shear zone (Rockwell et al., 2000), the Wasatch fault (e.g., McCalpin and Nishenko, 1996; Friedrich et al., 2003), the Dead Sea graben (Marco et al., 1996), the Oued Fodda fault in Algeria (Swan, 1988), and the Hebgen Lake fault in Montana (Zreda and Noller, 1998). In these cases, it appears that the temporal nature of the clusters themselves varies significantly. Faults with higher slip rates appear to display much shorter quiescent periods between clusters, on the order of two to three centuries in some cases (e.g., Sieh et al., 1989; Grant and Sieh, 1994), relative to faults with lower long-term slip rates, such as faults within the Eastern California shear zone or the Walker Lane, where quiescent periods tend to be significantly longer, on the order of 3–5 k.y. (e.g., Hecker et al., 1993; Rubin and Sieh, 1997; Rockwell et al., 2000). Where well documented, the time interval between events within earthquake clusters displays the same relationship, with faults with higher long-term slip rates, such as faults associated with the San Andreas system, displaying time intervals between clustered earthquakes on the decadal time scale (e.g., Sieh et al., 1989; Grant and Sieh, 1994) relative to faults with lower long-term slip rates, such as faults within the Eastern California shear zone, the Dead Sea graben, or the Oued Fodda fault (Algeria), which display time intervals between earthquake clusters on the order of hundreds or thousands of years (e.g., Swan, 1988; Marco et al., 1996; Rockwell et al., 2000; Friedrich et al., 2003).

Based on these findings, we suggest that the assessment of seismic hazard for the Wassuk Range fault might be simpler than for other major fault zones. The Wassuk Range normal fault has remained an active normal fault since at least ca. 15 Ma (Surpless et al., 2002; Stockli et al., 2002) with no significant strike-slip deformation or evidence for any change in fault position. Even within the present-day transtensional tectonic regime of the Walker Lane, there is no evidence for significant dextral slip along the fault zone (e.g., Wesnousky, 2005; Wesnousky et al., 2012; Dong et al., 2014), with strain instead accommodated by strike-slip faulting to the east (Dong et al., 2014), by hypothesized crustal block rotations between Lake Tahoe and the Wassuk Range (e.g., Unruh et al., 2003; Hammond et al., 2011; Wesnousky et al., 2012), and potentially by oblique-slip or strike-slip faulting in basins between the Wassuk Range and the Sierran range crest, to the west (e.g., Hammond et al., 2011, 2012; Bormann, 2013). In addition, there are no other major, tectonically active normal faults near the Wassuk Range fault system, with dextral faults to the east and relatively inactive normal faults to the west (not including the

Genoa fault or faults associated with the Lake Tahoe Basin; Fig. 1). This relative spatial isolation removes the likelihood that other nearby faults work in concert with the Wassuk fault to accommodate significant extensional strain release, with spatial changes in the loci of seismic activity transferred between subparallel fault systems (e.g., Lee et al., 2009; Petronis et al., 2009; Nagorsen-Rinke et al., 2013).

When these data are combined with the near match of geodetic data with geologic vertical strain rates since ca. 4 Ma, we posit that slip accommodated in future earthquakes should approximately match the time-averaged vertical displacement rates established by this and previous studies. Although data support a period of greater seismic activity between ca. 15.5 ka and 10.5 ka (Dong et al., 2014), there is no compelling evidence that the coseismic displacement rate associated with post–10 ka earthquakes is greater than the long-term average, so we hypothesize that the Wassuk fault is not in the midst of an earthquake cluster. Importantly, based on our analysis of long-term vertical displacement, with greater vertical displacement rates in the south relative to the north, we suggest that seismic risk should be slightly elevated proximal to the southern section of the fault relative to the northern section, consistent with seismic hazard maps generated by Petersen et al. (2008) and recent structural and thermochronologic data, which reveal that the highest post–4 Ma uplift rates in the Wassuk Range are associated with the Wassuk fault adjacent to Mount Grant (Gorinski et al., 2013).

Revised Kinematic Model of the Central Walker Lane

We suggest that the Wassuk Range has played and continues to play a significant role in the accommodation of extension across the Walker Lane at the latitude of Lake Tahoe, consistent with previous studies of the central Walker Lane and the Wassuk Range (e.g., Stewart, 1988; Surpless et al., 2002; Oldow, 2003; Wesnousky, 2005; Surpless, 2008; Wesnousky et al., 2012; Dong et al., 2014). The long-term rate of vertical displacement along the Wassuk fault is comparable to the most active fault systems in the western Basin and Range, including faults along the western margin of the Lake Tahoe Basin (0.85–1.7 mm/yr; Fig. 1; Kent et al., 2005; Brothers et al., 2009; Dingler et al., 2009; Rood et al., 2011) and the Genoa fault zone along the east flank of the Carson Range (2–3 mm/yr; Fig. 1; Ramelli et al., 1999). However, our results, when combined with new studies of the northern Eastern California shear zone–Walker Lane system (e.g., Hammond et al., 2011; Rood et al., 2011; Wesnousky et al., 2012; Carlson et al., 2013; Dong et al., 2014), support a revised model for system evolution over time. This model suggests spatially separate zones that alternate between areas dominated by clockwise crustal block rotations accommodated by NE- to E-trending faults to areas dominated by strain partitioning, with normal faults on the west and dextral faults on the east (Fig. 1).

To the north of the Wassuk Range, Cashman and Fontaine (2000) suggested that transtensional deformation has been accommodated by map-view clockwise rotations of crustal blocks in the Carson Sink area, with left-lateral fault displacements helping accommodate these rotations (Fig. 1). Their findings helped to explain the absence of significant dextral faults across the Walker Lane at that latitude, and it is worth noting that the normal faults between and including the Genoa fault and the Wassuk Range fault die out to the north at the same approximate latitude. More recently, Hammond et al. (2011) used block modeling based on geodetic data to show that clockwise block rotations have affected the Walker Lane at the latitude of Lake Tahoe and further north, consistent with geologic data, with the highest rates of deformation focused near the eastern and western margins of the northern Walker Lane. Other researchers (e.g., Oldow, 2003; Oldow et al., 2008) documented a similar combination of clockwise block rotations with left-lateral strike-slip faults and normal fault deformation in the Mina deflection region, and Carlson et al. (2013) constrained clockwise block rotations with left-lateral faults that have accommodated transtensional strain north of Mono Lake, adjacent to the Sierran range-front fault system (Fig. 1), at the latitude of the southernmost Wassuk fault. Thus, it appears that there are two zones where transtension has been accommodated by crustal fault block rotations across a significant percentage of the width of the Walker Lane: the first zone at the latitude of the Mina deflection, and the second zone to the north of the Wassuk Range, in the Carson Sink area (Fig. 1). Across these regions, faults are most commonly NE- to E-trending, at high angles to both Pacific–North American plate motion and most other normal and dextral faults throughout the Walker Lane–Eastern California shear zone (Fig. 1).

Northwest of the Carson Sink, dextral faults of the Pyramid Lake and Honey Lake region, subparallel to the plate boundary (Fig. 1), have accommodated most of the dextral shear associated with the plate boundary, with only minor extensional deformation (e.g., Faulds et al., 2005), and we suggest that for the belt of deformation defined by N- to NNW-trending normal faults and dextral faults, from Lake Tahoe on the west to the dextral fault complex (WLDF in Fig. 1) on the east (Fig. 1), transtensional deformation remains best explained by partitioning of strain between zones of extensional and dextral deformation. The spatial distribution of normal faults to the west of the northern Wassuk Range, including the Genoa fault, indicates that extensional strain has likely been shared over time between these east-dipping fault systems, with most extensional strain focused along the Wassuk fault, the Genoa fault, and faults within the Lake Tahoe Basin. However, displacements on the faults between the Genoa fault and the Wassuk fault die out to the south (Fig. 1), suggesting that more of the extensional deformation is taken up by the southern portion of the Wassuk fault system, perhaps explaining the higher long-term rates of vertical displacement along the southern Wassuk fault relative to the northernmost section of the fault (~1.1 mm/yr vs. ~0.6 mm/yr, respectively). The dextral fault system on the east (WLDF in Fig. 1) is along strike of the faults in the Pyramid Lake region, supporting a view where dextral strike-slip faults take up most of the plate-boundary–parallel motion in both zones.

In addition, Rood et al. (2011) showed that extensional deformation accommodated by the Sierran range-front fault system since ca. 20 ka increases from the southern extent of Figure 1 to the latitude of Mono Lake, suggesting that extension in the northern Eastern California shear zone is shared by a number of significant normal faults, but as these faults die out in the Mina deflection, the Sierran range front takes up a more significant component of extension across the Walker Lane–Eastern California shear zone. North of Mono Lake, rates of extension rapidly decrease and remain low as far north as at the southern termination of the Genoa fault, the northern extent of their study. Rood et al. (2011) posited that this extensional deformation is transferred eastward from the Sierran range front across the same region in which Carlson et al. (2013) showed clockwise block rotations. Although not discussed explicitly in Rood et al. (2011), this eastward shift in post–20 ka extension implies that the Wassuk Range fault system since ca. 20 ka has accommodated a significant portion of the total extension at this latitude of the Walker Lane. This hypothesis is consistent with the post–20 ka slip rates documented by Dong et al. (2014) for the Wassuk Range fault. However, our data suggest that if the Wassuk Range has indeed accommodated a greater percentage of the total displacement across the Walker Lane at this latitude, most of this strain was released in a brief period between ca. 15.5 ka and ca. 10.5 ka, with no evidence for high post–10 ka high vertical displacement rates.

The geomorphic expression of normal faults and basins and studies of dip-slip displacements at this latitude (e.g., Ramelli et al., 1999; Surpless et al., 2002; Schweickert et al., 2004; Kent et al., 2005; Surpless, 2008; Cashman et al., 2009) support a model in which most of the extension has been accommodated by the fault systems along the Sierran range front and by the Wassuk Range fault system since the late Pliocene, with much lower rates of deformation accommodated between those fault systems. It is possible that a small percentage of dextral shear is accommodated by fault systems along the Sierran range-front system (e.g., Unruh et al., 2003; Hammond et al., 2011) or by other fault systems to the west of the Wassuk Range (e.g., Wesnousky et al., 2012), but there is no geologic evidence or historical seismicity that would support significant dextral deformation or block rotations across this region of the Walker Lane. If future studies do establish either crustal block rotations or dextral deformation across this zone, this model of strain partitioning would need to be revised.

CONCLUSIONS

We suggest that the Wassuk Range fault zone has slipped at a constant rate of 0.75–1.0 mm/yr since at least ca. 4 Ma, with the likely cluster of earthquakes along the Wassuk fault between ca. 15.5 ka and ca. 10.5 ka triggered by rapid transgression of the ancestral Lake Lahontan, a nontectonic stressor. Because the post–10 ka vertical displacement rate is so similar to the long-term rate, we suggest that the cluster was anomalous in the fault's slip history and should not be used to suggest Wallace-type behavior. Thus, we posit that the Wassuk Range exhibits a slip history more compatible with slip-predictable Reid-type fault behavior, which contrasts with the behaviors of many other faults, where researchers have established relatively constant slip rates over long time scales punctuated by relatively brief periods of higher seismic slip (e.g., Swan, 1988; Sieh et al., 1989; Hecker et al., 1993; Grant and Sieh, 1994; Marco et al., 1996; Rubin and Sieh, 1997; Rockwell et al., 2000; Friedrich et al., 2003). However, we suggest that nontectonic stressors, such as hydrologic loading or unloading on the hanging wall of normal faults, may influence temporal variations in rate of strain release along other major fault systems worldwide.

The unusual behavior of the Wassuk Range might be explained by the relative isolation of the fault system relative to major normal faults across the Walker Lane. In the cases of most major faults worldwide, the faults analyzed were part of systems with relatively close, subparallel faults with similar senses of and magnitudes of slip, perhaps affecting the behavior of individual faults within those systems. In these systems, it is likely that each fault's slip history recorded periods when individual faults accommodated greater or lesser percentages of the system's total strain release. In the case of the Wassuk fault, it is possible that the lack of other major normal faults in close proximity has resulted in a single fault that accommodates a significant percentage of Walker Lane extensional strain, with strain release that has remained relatively constant since ca. 4 Ma.

If the Wassuk fault does indeed follow Reid-type behavior, we suggest that seismic hazard assessment for the Wassuk fault is perhaps simpler than for other major faults. The data presented here also imply that a range of possible vertical displacement histories characterizes major fault zones, even when compared to similar fault zones from the same tectonic setting (e.g., Rockwell et al., 2000; Friedrich et al., 2003), with assessment of seismic hazard necessarily informed by the relative timing of, or lack of, earthquake clusters.

We also propose a revised model of the central Walker Lane that integrates these results with recent ideas about how transtensional deformation has been accommodated across the Walker Lane–Eastern California shear zone north of the Mina deflection. For the Walker Lane north of the northern Eastern California shear zone, we suggest that transtensional deformation has been accommodated by spatially segregated zones alternately dominated by clockwise crustal block rotations, by partitioning of strain between normal and dextral fault systems, and by possible, but not yet documented, intrabasinal dextral faults.

ACKNOWLEDGMENTS

Special thanks go to Steve Wesnousky for his thorough and insightful review of the initial draft of this manuscript. Also, thanks go to Whitney Behr for helpful discussion about cosmogenic nuclide exposure age dating, and thanks go to Daniel Stockli for discussion of hydrologic loading of fault systems. We also thank Bill Hammond, an anonymous reviewer, and the *GSA Bulletin*'s editorial staff for their constructive feedback. Thanks are also due to John Michael Bentz, Brett Mays, and Kristine Quiroz Purcell, Trinity University undergraduates who assisted in field investigations and subsequent analysis. Thanks go to Tony Perez and Denise Wilson, who aided in the planning and execution of field work. Field work, transportation, and laboratory analyses were funded by the Trinity University Department of Geosciences.

REFERENCES CITED

Adams, K.D., and Wesnousky, S.G., 1998, Shoreline processes and the age of the Lake Lahontan highstand in the Jessup embayment, Nevada: Geological Society of America Bulletin, v. 110, p. 1318–1332, doi:10.1130/0016-7606(1998)110<1318:SPATAO>2.3.CO;2.

Adams, K.D., Wesnousky, S., and Bills, B., 1999, Isostatic rebound, active faulting, and potential geomorphic effects in the Lake Lahontan basin, Nevada and California: Geological Society of America Bulletin, v. 111, p. 1739–1756, doi:10.1130/0016-7606(1999)111<1739:IRAFAP>2.3.CO;2.

Argus, D.F., and Gordon, R.G., 1991, Current Sierra Nevada–North America motion from very long baseline interferometry—Implications for the kinematics of the western United States: Geology, v. 19, p. 1085–1088, doi:10.1130/0091-7613(1991)019<1085:CSNNAM>2.3.CO;2.

Atwater, T., and Stock, J., 1998, Pacific–North America plate tectonics of the Neogene of the southwestern United States; an update: International Geology Review, v. 40, p. 375–402, doi:10.1080/00206819809465216.

Balco, G., Stone, J.O., Lifton, N.A., and Dunai, T.J., 2008, A complete and easily accessible means of calculating surface exposure ages or erosion rates from ^{10}Be and ^{26}Al measurements: Quaternary Geochronology, v. 3, p. 174–195, doi:10.1016/j.quageo.2007.12.001.

Behr, W.M., Rood, D., Fletcher, K., Guzman, N., Finkel, R., Hanks, T., Hudnut, K., Kendrick, K., Platt, J., Sharp, W., Weldon, R., and Yule, J., 2010, Uncertainties in slip-rate estimates for the Mission Creek strand of the southern San Andreas fault at Biskra Palms Oasis, southern California: Geological Society of America Bulletin, v. 122, p. 1360–1377, doi:10.1130/B30020.1.

Bennett, R.A., Wernicke, B.P., Niemi, N.A., Friedrich, A.M., and Davis, J.L., 2003, Contemporary strain rates in the northern Basin and Range Province from GPS data: Tectonics, v. 22, 1008, doi:10.1029/2001TC001355.

Benson, L.V., 1991, Timing of the last highstand of Lake Lahontan: Journal of Paleolimnology, v. 5, p. 115–126, doi:10.1007/BF00176873.

Benson, L.V., 1993, Factors affecting ^{14}C ages of lacustrine carbonates: Timing and duration of the last highstand lake in the Lahontan Basin: Quaternary Research, v. 39, p. 163–174, doi:10.1006/qres.1993.1020.

Benson, L.V., and Mifflin, M.D., 1986, Reconnaissance Bathymetry of Basins Occupied by Pleistocene Lake Lahontan, Nevada and California: U.S. Geological Survey Water-Resources Investigations Report 85-4262, 14 p.

Benson, L.V., Currey, D.R., Lao, Y., and Hostetler, S.W., 1992, Lake-size variations in the Lahontan and Bonneville basins between 13,000 and 9,000 ^{14}C yr B.P.: Palaeogeography, Palaeoclimatology, Palaeoecology, v. 95, p. 19–32, doi:10.1016/0031-0182(92)90162-X.

Benson, L.V., Kashgarian, M., and Rubin, M., 1995, Carbonate deposition, Pyramid Lake subbasin, Nevada: 2. Lake levels and polar jet stream positions reconstructed from radiocarbon ages and elevations of carbonates (tufas) deposited in the Lahontan basin: Palaeogeography, Palaeoclimatology, Palaeoecology, v. 117, p. 1–30, doi:10.1016/0031-0182(94)00103-F.

Bills, B.G., Adams, K.D., and Wesnousky, S.G., 2007, Viscosity structure of the crust and upper mantle in western Nevada from isostatic rebound patterns of the late Pleistocene Lake Lahontan high shoreline: Journal of Geophysical Research, v. 112, B06405, doi:10.1029/2005JB003941.

Blard, P.H., Lave, J., Pik, R., Wagnon, P., and Bourles, D., 2007, Persistence of full glacial conditions in the central Pacific until 15,000 years ago: Nature, v. 449, no. 7162, p. 591–594, doi:10.1038/nature06142.

Bormann, J.M., 2013, New Insights into Strain Accumulation and Release in the Central and Northern Walker Lane, Pacific–North American Plate Boundary, California and Nevada, USA [Ph.D. thesis]: Reno, Nevada, University of Nevada, 150 p.

Bormann, J.M., Surpless, B.E., Caffee, M.W., and Wesnousky, S.G., 2012, Holocene earthquakes and late Pleistocene slip-rate estimates on the Wassuk Range fault zone, Nevada: Bulletin of the Seismological Society of America, v. 102, p. 1884–1891, doi:10.1785/0120110287.

Born, S.M., 1972, Late Quaternary History, Deltaic Sedimentation, and Mudlump Formation at Pyramid Lake, Nevada: Reno, Nevada, Center for Water Resources, Desert Research Institute, 97 p.

Briggs, R.W., Wesnousky, S.G., and Adams, K.D., 2005, Late Pleistocene and late Holocene lake highstands in the Pyramid Lake subbasin of Lake Lahontan, Nevada, USA: Quaternary Research, v. 64, p. 257–263, doi:10.1016/j.yqres.2005.02.011.

Brothers, D.S., Kent, G.M., Driscoll, N.W., Smith, S.B., Karlin, R., Dingler, J.A., Harding, A.J., Seitz, G.G., and Babcock, J.M., 2009, New constraints on deformation, slip rate, and timing of the most recent earthquake on the West Tahoe–Dollar Point fault, Lake Tahoe Basin, California: Bulletin of the Seismological Society of America, v. 99, p. 499–519, doi:10.1785/0120080135.

Bull, W., 2007, Tectonic Geomorphology of Mountains: A New Approach to Paleoseismology: Hoboken, New Jersey, Wiley Publishing, 328 p.

Burchfiel, B.C., Cowan, D.S., and Davis, G.A., 1992, Tectonic overview of the Cordilleran orogen in the western United States, *in* Buchfiel, B.C., Lipman, P.W., and Zoback, M.L., eds., The Cordilleran Orogen; Conterminous United States: Boulder, Colorado, Geological Society of America, Geology of North America, v. G3, p. 407–479.

Burger, H.R., 1992, Exploration Geophysics of the Shallow Subsurface: Upper Saddle River, New Jersey, Prentice Hall Publishing, 489 p.

Carder, D.S., 1970, Reservoir loading and local earthquakes, *in* Adams, W., ed., Engineering Geology Case Histories: Boulder, Colorado, Geological Society of America, p. 51–61.

Carlson, C.W., Pluhar, C.J., Glen, J.M.G., and Farner, M.J., 2013, Kinematics of the west-central Walker Lane: Spatially and temporally variable rotations evident in the late Miocene Stanislaus Group: Geosphere, v. 9, p. 1530–1551, doi:10.1130/GES00955.1.

Cashman, P.H., and Fontaine, S.A., 2000, Strain partitioning in the northern Walker Lane, western Nevada and northeastern California: Tectonophysics, v. 326, p. 111–130, doi:10.1016/S0040-1951(00)00149-9.

Cashman, P.H., Trexler, J.H., Muntean, T., Faulds, J.E., Louie, J.N., and Oppliger, G.L., 2009, Neogene tectonic evolution of the Sierra Nevada–Basin and Range transition zone at the latitude of Carson City, Nevada, *in* Oldow, J.S., and Cashman, P.H., eds., Late Cenozoic Structure and Evolution of the Great Basin–Sierra Nevada Transition: Geological Society of America Special Paper 447, p. 171–188, doi:10.1130/2009.2447(10).

Chang, W., Smith, R.B., Meertens, C.M., and Harris, R.A., 2006, Contemporary deformation of the Wasatch fault, Utah, from GPS measurements with implications for interseismic fault behavior and earthquake hazard: Observations and kinematic analysis: Journal of Geophysical Research, v. 111, B11405, doi:10.1029/2006JB004326.

Cooke, R.U., and Mason, P., 1973, Desert Knolls pediment and associated landforms in the Mojave Desert, California: Revue de Geomorphologie Dynamique, v. 20, p. 71–78.

Cowgill, E., Gold, R.D., Xuanhua, C., Xiao-Feng, W., Arrowsmith, J.R., and Southon, J., 2009, Low Quaternary slip rate reconciles geodetic and geologic rates along the Altyn Tagh fault, northwestern Tibet: Geology, v. 37, p. 647–650, doi:10.1130/G25623A.1.

DeMets, C., Gordon, R.G., Argus, D.F., and Stein, S., 1994, Effect of recent revisions to the geomagnetic reversal time scale on estimates of current plate motions: Geophysical Research Letters, v. 21, p. 2191–2194, doi:10.1029/94GL02118.

Demsey, K., 1987, Holocene Faulting and Tectonic Geomorphology along the Wassuk Range, West-Central Nevada [M.S. thesis]: Tucson, Arizona, University of Arizona, 64 p.

dePolo, C., and Anderson, J., 2000, Estimating the slip rates of normal faults in the Great Basin, USA: Basin Research, v. 12, p. 227–240, doi:10.1046/j.1365-2117.2000.00131.x.

Dilles, J.H., 1993, Cenozoic and normal and strike-slip faults in the northern Wassuk Range, western Nevada, *in* Craig, S.D., ed., Structure, Tectonics, and Mineralization of the Walker Lane, Walker Lane Symposium Proceedings: Reno, Nevada, Geological Society of Nevada, p. 114–136.

Dingler, J., Kent, G., Driscoll, N., Babcock, J., Harding, A., Seitz, G., Karlin, B., and Goldman, C., 2009, A high-resolution seismic CHIRP investigation of active normal faulting across Lake Tahoe Basin, California-Nevada: Geological Society of America Bulletin, v. 121, p. 1089–1107, doi:10.1130/B26244.1.

Dixon, T.H., Stefano, R., Lee, J., and Reheis, M.C., 1995, Constraints on present-day Basin and Range deformation from space geodesy: Tectonics, v. 14, p. 755–772, doi:10.1029/95TC00931.

Dixon, T.H., Norabuena, E., and Hotaling, L., 2003, Paleoseismology and global positioning system: Earthquake-cycle effects and geodetic versus geologic fault slip rates in the Eastern California shear zone: Geology, v. 31, p. 55–58, doi:10.1130/0091-7613(2003)031<0055:PAGPSE>2.0.CO;2.

Dohrenwend, J.C., 1982, Tectonic control of pediment distribution in the western Great Basin: Geological Society of America Abstracts with Programs, v. 14, p. 161.

Dohrenwend, J.C., and Parsons, A.J., 1994, Pediments in arid environments, *in* Abrahams, A.D., and Parsons, A.J., eds., Geomorphology of Desert Environments: London, Chapman and Hall, p. 321–353.

Dong, S., Ucarkus, G., Wesnousky, S., Maloney, J., Kent, G., Driscoll, N., and Baskin, R., 2014, Strike-slip faulting along the Wassuk Range of the northern Walker Lane, Nevada: Geosphere, v. 10, p. 40–48, doi:10.1130/GES00912.1.

Ellis, M., Densmore, A., and Anderson, R., 1999, Development of mountainous topography in the Basin and Ranges, USA: Basin Research, v. 11, p. 21–41, doi:10.1046/j.1365-2117.1999.00087.x.

Faulds, J.E., Henry, C.D., and Hinz, N.H., 2005, Kinematics of the northern Walker Lane: An incipient transform fault along the Pacific–North American plate boundary: Geology, v. 33, p. 505–508, doi:10.1130/G21274.1.

Foy, T.A., Frankel, K.L., Lifton, Z.M., Johnson, C.W., and Caffee, M.W., 2012, Distributed extensional deformation in a zone of right-lateral shear: Implications for geodetic versus geologic rates of deformation in the Eastern California shear zone–Walker Lane: Tectonics, v. 31, TC4008, doi:10.1029/2011TC002930.

Friedrich, A.M., Wernicke, B.P., Niemi, N.A., Bennett, R.A., and Davis, J.L., 2003, Comparison of geodetic and geologic data from the Wasatch region, Utah, and implications for the spectral character of Earth deformation at periods of 10 to 10 million years: Journal of Geophysical Research, v. 108, p. 2199, doi:10.1029/2001JB000682.

Garvin, C.D., Hanks, T.C., Finkel, R.C., and Heimsath, A.M., 2005, Episodic incision of the Colorado River in Glen Canyon, Utah: Earth Surface Processes and Landforms, v. 30, p. 973–984, doi:10.1002/esp.1257.

Gorinski, K., Stockli, D.F., and Walker, J.D., 2013, Thermochronometrically constrained anatomy and evolution of a Miocene extensional accommodation zone and tilt domain boundary: The southern Wassuk Range, Nevada: Tectonics, v. 32, p. 516–539, doi:10.1002/tect.20044.

Gosse, J.C., and Phillips, F.M., 2001, Terrestrial in situ cosmogenic nuclides: Theory and application: Quaternary Science Reviews, v. 20, p. 1475–1560, doi:10.1016/S0277-3791(00)00171-2.

Grant, L., and Sieh, K., 1994, Paleoseismic evidence of clustered earthquakes on the San Andreas fault in the Carrizo Plain, California: Journal of Geophysical Research, v. 99, p. 6819–6841, doi:10.1029/94JB00125.

Grosfils, E.B., Schultz, R.A., and Kroeger, G., 2003, Geophysical exploration within northern Devils Lane graben, Canyonlands National Park, Utah: Implications for sediment thickness and tectonic evolution: Journal of Structural Geology, v. 25, p. 455–467, doi:10.1016/S0191-8141(02)00040-8.

Guilderson, T.P., Southon, J.R., and Brown, T.A., 2003, High-precision AMS ^{14}C results on TIRI/FIRI turbidite: Radiocarbon, v. 45, p. 75–80.

Hager, B.H., Lyzenga, G.A., Donnellan, A., and Dong, D., 1999, Reconciling rapid strain accumulation with deep seismogenic fault planes in the Ventura Basin, California: Journal of Geophysical Research, v. 104, p. 25,207–25,219, doi:10.1029/1999JB900184.

Hammond, W., and Thatcher, W., 2007, Crustal deformation across the Sierra Nevada, northern Walker Lane, Basin and Range transition, western United States measured with GPS, 2000–2004: Journal of Geophysical Research–Solid Earth Planets, v. 112, B05411, doi:10.1029/2006JB004625.

Hammond, W., Blewitt, G., and Kreemer, C., 2011, Block modeling of crustal deformation of the northern Walker Lane and Basin and Range from GPS velocities: Journal of Geophysical Research–Solid Earth Planets, v. 116, B04402, doi:10.1029/2010JB007817.

Hammond, W., Kreemer, C., Blewitt, G., and Bormann, J.N., 2012, GPS measurement of active crustal deformation of the Lake Tahoe Basin and vicinity, *in* Seitz, G., comp., Friends of the Pleistocene Field Trip Guidebook: Menlo Park, California, California Geological Survey, p. 123–130.

Hanks, T.C., Lucchitta, I., Davis, S.W., Davis, M.E., Lefton, S.A., and Garvin, C.D., 2001, The Colorado River and the age of Glen Canyon, *in* Young, R.A., and Spamer, E.E., eds., The Colorado River: Origin and Evolution: Grand Canyon, Arizona, Grand Canyon Monograph 12, p. 129–133.

Hearn, E.H., and Humphreys, E.D., 1998, Kinematics of the southern Walker Lane belt and motion of the Sierra Nevada block, California: Journal of Geophysical Research, v. 103, p. 27,033–27,049, doi:10.1029/98JB01390.

Hecker, S., Fumal, T.E., Powers, T.J., Hamilton, J.C., Garvin, C.D., and Schwartz, D.P., 1993, Late Pleistocene–Holocene behavior of the Homestead Valley fault segment—1992 Landers, CA surface rupture: Eos, American Geophysical Union, v. 74, Fall supplement, p. 612.

Heyman, J., Stroeven, A.P., Harbor, J.M., and Caffee, M.W., 2011, Too young or too old: Evaluating cosmogenic exposure dating based on an analysis of compiled boulder exposure ages: Earth and Planetary Science Letters, v. 302, p. 71–80, doi:10.1016/j.epsl.2010.11.040.

Hoeft, J.S., and Frankel, K.L., 2010, Temporal variations in extension rate along the Lone Mountain fault and strain partitioning in the Eastern California shear zone–Walker Lane: Geosphere, v. 6, p. 917–936, doi:10.1130/GES00603.1.

House, P.K., and Adams, K.D., 2009, Preliminary Geologic Map of the Southern Part of the Lower Walker River Area, Mineral County, Nevada: Nevada Bureau of Mines and Geology Open-File Report 09-13, scale 1:24,000.

Ichinose, G.A., Smith, K.D., and Anderson, J.G., 1998, Moment tensor solutions of the 1994 to 1996 Double Spring Flat, Nevada, earthquake sequence and implications for local tectonic models: Bulletin of the Seismological Society of America, v. 88, p. 1363–1378.

Jewell, P.W., and Bruhn, R.L., 2013, Evaluation of Wasatch fault segmentation and slip rates using Lake Bonneville shorelines: Journal of Geophysical Research, v. 118, p. 2528–2543, doi:10.1002/jgrb.50174.

Kent, G.M., Babcock, J.M., Driscoll, N.W., Harding, A.J., Dingler, J.A., Seitz, G.G., Gardner, J.V., Mayer, L.A., Goldman, C.R., Heyvaert, A.C., Richards, R.C., Karlin, R., Morgan, C.W., Gayes, P.T., and Owen, L.A., 2005, 60 k.y. record of extension across the western boundary of the Basin and Range Province: Estimate of slip rates from offset shoreline terraces and a catastrophic slide beneath Lake Tahoe: Geology, v. 33, p. 365–368, doi:10.1130/G21230.1.

Kirby, E., Whipple, K., and Harkins, N., 2008, Topography reveals seismic hazard: Nature Geoscience, v. 1, p. 485–487, doi:10.1038/ngeo265.

Kohl, C.P., and Nishiizumi, K., 1992, Chemical isolation of quartz for measurement of in situ–produced cosmogenic nuclides: Geochimica et Cosmochimica Acta, v. 56, p. 3583–3587, doi:10.1016/0016-7037(92)90401-4.

Kreemer, C., Blewitt, G., and Hammond, W.C., 2009, Geodetic constraints on contemporary deformation in the northern Walker Lane: 2. Velocity and tensor strain rate analysis, *in* Oldow, J., and Cashman, P., eds., Late Cenozoic Structure and Evolution of the Great Basin–Sierra Nevada Transition: Geological Society

of America Special Paper 447, p. 33–54, doi:10.1130/2009.2447(03).

Lal, D., 1991, Cosmic ray labeling of erosion surfaces: In situ production rates and erosion models: Earth and Planetary Science Letters, v. 104, p. 424–439, doi:10.1016/0012-821X(91)90220-C.

Lay, T., and Wallace, T.C., 1995, Modern Global Seismology: San Diego, California, Academic Press, 521 p.

Lee, J., Spencer, J., and Owen, L., 2001, Holocene slip rates along the Owens Valley fault, California: Implications for the recent evolution of the Eastern California shear zone: Geology, v. 29, p. 819–822, doi:10.1130/0091-7613(2001)029<0819:HSRATO>2.0.CO;2.

Lee, J., Garwood, J., Stockli, D.F., and Gosse, J., 2009, Quaternary faulting in Queen Valley, California–Nevada: Implications for kinematics of fault-slip transfer in the Eastern California shear zone–Walker Lane belt: Geological Society of America Bulletin, v. 121, p. 599–614, doi:10.1130/B26352.1.

Ludington, S., McKee, E., Cox, D., Moring, B., and Leonard, K., 1996, Pre-Tertiary Geology of Nevada: U.S. Geological Survey Open-File Report 96-2, scale 1:1,000,000.

Marco, S., Stein, M., Agnon, A., and Ron, H., 1996, Long-term earthquake clustering: A 50,000-year paleoseismic record in the Dead Sea graben: Journal of Geophysical Research, v. 101, p. 6179–6191, doi:10.1029/95JB01587.

McCalpin, J., 1999, New age control from the Wasatch fault megatrench of 1999: Geological Society of America Abstracts with Programs, v. 34, A12, p. 1999.

McCalpin, J., and Nelson, C., 2000, Long Recurrence Records from the Wasatch Fault, Utah: Reston, Virginia, U.S. Geological Survey, NEHRP Annual Report, 61 p.

McCalpin, J., and Nelson, C., 2001, Long Recurrence Records from the Wasatch Fault Zone, Utah, Program Element II: Evaluate Urban Hazard and Risk: Crestone, Colorado, U.S. Geological Survey, Final Technical Report, Contract 01HQGR0029, 48 p.

McCalpin, J., and Nishenko, S., 1996, Holocene paleoseismicity, temporal clustering, and probabilities of future large (M > 7) earthquakes on the Wasatch fault zone, Utah: Journal of Geophysical Research, v. 101, p. 6233–6253, doi:10.1029/95JB02851.

McGarr, A., Simpson, D., and Seeber, L., 2002, 40 case histories of induced and triggered seismicity: International Geophysics, v. 81, p. 647–661, doi:10.1016/S0074-6142(02)80243-1.

Murphy, J.J., Watkinson, A.J., and Oldow, J.S., 2009, Graphical analysis of divergence between GPS velocity and strain trajectory within the Walker Lane, Nevada, *in* Oldow, J., and Cashman, P., eds., Late Cenozoic Structure and Evolution of the Great Basin–Sierra Nevada Transition: Geological Society of America Special Paper 447, p. 55–70, doi:10.1130/2009.2447(03).

Nagorsen-Rinke, S., Lee, J., and Calvert, A., 2013, Pliocene sinistral slip across the Adobe Hills, eastern California–western Nevada: Kinematics of fault slip transfer across the Mina deflection: Geosphere, v. 9, p. 37–53, doi:10.1130/GES00825.1.

Nishiizumi, K., Imamura, M., Caffee, M.W., Southon, J.R., Finkel, R.C., and McAninch, J., 2007, Absolute calibration of ^{10}Be AMS standards: Nuclear Instruments and Methods, Section B, v. 258, p. 403–413, doi:10.1016/j.nimb.2007.01.297.

Oldow, J.S., 2003, Active transtensional boundary zone between the western Great Basin and Sierra Nevada block, western U.S. Cordillera: Geology, v. 31, p. 1033–1036, doi:10.1130/G19838.1.

Oldow, J.S., Balley, A.W., Ave Lallemant, H.G., and Leeman, W.P., 1989, Phanerozoic evolution of the North American Cordillera (United States and Canada), *in* Bally, A.W., and Palmer, A.R., eds., The Geology of North America: An Overview: Boulder, Colorado, Geological Society of America, Geology of North America, v. A, p. 139–232.

Oldow, J.S., Aiken, C.L.V., Ferguson, J.F., Hare, J.L., and Hardyman, R.F., 2001, Active displacement transfer and differential motion between tectonic blocks within the central Walker Lane, western Great Basin: Geology, v. 29, p. 19–22, doi:10.1130/0091-7613(2001)029<0019:ADTADB>2.0.CO;2.

Oldow, J.S., Geissman, J.W., and Stockli, D.F., 2008, Evolution and strain reorganization within late Neogene structural stepovers linking the central Walker Lane and northern Eastern California shear zone, western Great Basin: International Geology Review, v. 50, p. 270–290, doi:10.2747/0020-6814.50.3.270.

Olig, S.S., McDonald, G., Black, B.D., DuRoss, C.B., Lund, W.R., Hylland, M., Simon, D.B., Giraud, R.E., and Christenson, G.E., 2011, Extending the paleoseismic record of the Provo segment of the Wasatch fault zone, Utah: Final Technical Report submitted to the U.S. Geological Survey National Earthquake Hazards Reduction Program, Contract 02HQGR0109, Oakland, California, 100 p.

Oskin, M., Perg, L., Blumentritt, D., Mukhopadhyay, S., and Iriondo, A., 2007, Slip rate of the Calico fault: Implications for geologic versus geodetic rate discrepancy in the Eastern California shear zone: Journal of Geophysical Research, v. 112, B03402, doi:10.1029/2006JB004451.

Owen, L.A., Frankel, K.L., Knott, J.R., Reynhout, S., Finkel, R.C., Dolan, J.F., and Lee, J., 2011, Beryllium-10 terrestrial cosmogenic nuclide surface exposure dating of Quaternary landforms in Death Valley: Geomorphology, v. 125, p. 541–557, doi:10.1016/j.geomorph.2010.10.024.

Peltzer, G., Crampe, F., Hensley, S., and Rosen, P., 2001, Transient strain accumulation and fault interaction in the Eastern California shear zone: Geology, v. 29, p. 975–978, doi:10.1130/0091-7613(2001)029<0975:TSAAFI>2.0.CO;2.

Petersen, M.D., Frankel, A.D., Harmsen, S.C., Mueller, C.S., Haller, K.M., Wheeler, R.L., Wesson, R.L., Zeng, Y., Boyd, O.S., Perkins, D.M., Luco, N., Field, E.H., Wills, C.J., and Rukstales, K.S., 2008, Documentation for the 2008 Update of the United States National Seismic Hazard Maps: U.S. Geological Survey Open-File Report 2008-1128, 61 p.

Petit, C., Gunnell, Y., Gonga-Saholiariliva, N., Meyer, B., and Se'guinot, J., 2009a, Faceted spurs at normal fault scarps: Insights from numerical modeling: Journal of Geophysical Research, v. 114, B05403, doi:10.1029/2008JB005955.

Petit, C., Meyer, B., Gunnell, Y., Jolivet, M., San'kov, V., Strak, V., and Gonga-Saholiariliva, N., 2009b, Height of faceted spurs, a proxy for determining long-term throw rates on normal faults: Evidence from the North Baikal Rift System, Siberia: Tectonics, v. 28, TC6010, doi:10.1029/2009TC002555.

Petronis, M.S., Geissman, J.W., Oldow, J.S., and McIntosh, W.C., 2009, Late Miocene to Pliocene vertical-axis rotation attending development of the Silver Peak–Lone Mountain displacement transfer zone, west-central Nevada, *in* Oldow, J.S., and Cashman, P.H., eds., Late Cenozoic Structure and Evolution of the Great Basin–Sierra Nevada Transition Zone: Geological Society of America Special Paper 447, p. 215–253, doi:10.1130/2009.2447(12).

Pollitz, F.F., McCrory, P., Svarc, J., and Murray, J., 2008, Dislocation models of interseismic deformation in the western United States: Journal of Geophysical Research, v. 113, B04413, doi:10.1029/2007JB005174.

Putkonen, J., and Swanson, T., 2003, Accuracy of cosmogenic ages for moraines: Quaternary Research, v. 59, no. 2, p. 255–261, doi:10.1016/S0033-5894(03)00006-1.

Ramelli, A.R., Bell, J.W., dePolo, C.M., and Yount, J.C., 1999, Large-magnitude, late Holocene earthquakes on the Genoa fault, west-central Nevada and eastern California: Bulletin of the Seismological Society of America, v. 89, p. 1458–1472.

Reid, H.F., 1910, The California earthquake of April 18, 1906: The mechanics of the earthquake: Sacramento, California, California State Earthquake Investigation Committee, Report of the (California) State Earthquake Investigation Commission, Volume 2, Publication 87, 192 p.

Rockwell, T., Lindvall, S., Herzberg, M., Murbach, D., Dawson, T., and Berger, G., 2000, Paleoseismology of the Johnson Valley, Kickapoo, and Homestead Valley faults: Clustering of earthquakes in the Eastern California shear zone: Journal of Geophysical Research, v. 90, p. 1200–1236.

Roeloffs, E.A., 1988, Fault stability changes induced beneath a reservoir with cyclic variations in water level: Journal of Geophysical Research, v. 93, p. 2107–2124, doi:10.1029/JB093iB03p02107.

Rood, D.H., Burbank, D.W., and Finkel, R.C., 2011, Chronology of glaciations in the Sierra Nevada, California, from ^{10}Be surface exposure dating: Quaternary Science Reviews, v. 30, p. 646–661, doi:10.1016/j.quascirev.2010.12.001.

Rubin, C.M., and Sieh, K., 1997, Long dormancy, low slip rate, and similar slip-per-event for the Emerson fault, Eastern California shear zone: Journal of Geophysical Research, v. 102, p. 15,319–15,333, doi:10.1029/97JB00265.

Savage, J.C., 2000, Viscoelastic-coupling model for the earthquake cycle driven from below: Journal of Geophysical Research, v. 105, p. 25,525–25,532, doi:10.1029/2000JB900276.

Scholz, C., 1990, The Mechanics of Earthquakes and Faulting: New York, Cambridge University Press, 461 p.

Schweickert, R.A., Lahren, M.M., Smith, K.D., Howle, J.F., and Ichinose, G., 2004, Transtensional deformation in the Lake Tahoe region, California and Nevada, USA: Tectonophysics, v. 392, p. 303–323, doi:10.1016/j.tecto.2004.04.019.

Sella, G.F., Dixon, T.H., Mao, A., 2002, REVEL: A model for recent plate velocities from space geodesy: Journal of Geophysical Research, v. 107, p. ETG 11-1–ETG 11-30, doi:10.1029/2000JB000033.

Sharma, P., Bourgeois, M., Elmore, D., Granger, D., Lipschutz, M.E., Ma, X., Miller, T., Mueller, K., Rickey, G., Simms, P., and Vogt, S., 2000, PRIME Lab AMS performance, upgrades and research applications: Nuclear Instruments and Methods, Section B, v. 172, p. 112–123, doi:10.1016/S0168-583X(00)00132-4.

Sheehan, T.P., 2007, Evolution of Neogene Fault Populations in Northern Owens Valley, California and Implications for the Eastern California Shear Zone [Ph.D. thesis]: New Orleans, Louisiana, Tulane University, 203 p.

Shimazaki, K., and Nakata, T., 1980, Time-predictable recurrence model for large earthquakes: Geophysical Research Letters, v. 7, p. 279–282, doi:10.1029/GL007i004p00279.

Sieh, K., Stuiver, M., and Brillinger, D., 1989, A more precise chronology of earthquakes produced by the San Andreas fault in southern California: Journal of Geophysical Research, v. 94, p. 603–623, doi:10.1029/JB094iB01p00603.

Simpson, D.W., and Negmatullaev, S., 1981, Induced seismicity at Nurek Reservoir, Tadjikistan, USSR: Bulletin of the Seismological Society of America, v. 71, p. 1561–1586.

Simpson, D.W., Leith, W.S., and Scholz, C.H., 1988, Two types of reservoir induced seismicity: Bulletin of the Seismological Society of America, v. 78, p. 2025–2040.

Sonder, L.J., and Jones, C.H., 1999, Western United States extension; how the west was widened: Annual Review of Earth and Planetary Sciences, v. 27, p. 417–462, doi:10.1146/annurev.earth.27.1.417.

Stewart, J.H., 1988, Tectonics of the Walker Lane belt, western Great Basin—Mesozoic and Cenozoic deformation in a zone of shear, *in* Ernst, W.G., ed., Metamorphism and Crustal Evolution of the Western United States: Upper Saddle River, New Jersey, Prentice Hall, Rubey Volume VII, p. 683–713.

Stewart, J.H., and Carlson, J.E., 1978, Geologic Map of Nevada: Nevada Bureau of Mines and Geology Map 57, scale 1:500,000.

Stockli, D.F., Surpless, B.E., and Dumitru, T.A., 2002, Thermochronological constraints on the timing and magnitude of Miocene and Pliocene extension in the central Wassuk Range, western Nevada: Tectonics, v. 21, p. 10-1–10-19, doi:10.1029/2001TC001295.

Stone, J.O., 2000, Air pressure and cosmogenic isotope production: Journal of Geophysical Research, v. 105, p. 23,753–23,759, doi:10.1029/2000JB900181.

Surpless, B.E., 2008, Modern strain localization in the central Walker Lane, western United States: Implications for the evolution of intraplate deformation in transtensional settings: Tectonophysics, v. 457, p. 239–253, doi:10.1016/j.tecto.2008.07.001.

Surpless, B.E., 2010a, Geologic Map of the Central Wassuk Range, western Nevada: Geological Society of America Map and Chart Series MCH098, scale 1:24,000, doi:10.1130/2010.MCH098.

Surpless, B.E., 2010b, Evolution of a segmented fault system: A reconnaissance study of the Reese River–Penrod Canyon fault system, northern Wassuk Range, *in* Wesnousky, S., comp., Friends of the Pleistocene Field Trip Guidebook: Reno, Nevada, University of Nevada at Reno, p. 59–65.

Surpless, B.E., 2011, Cenozoic tectonic evolution of the central Wassuk Range, western Nevada, USA.: International Geology Review, v. 54, no. 5, p. 547–571, doi:10.1080/00206814.2010.548117.

Surpless, B.E., and Bentz, J.M., 2011, Fundamental segmentation of the northern and central Wassuk Range, Nevada: Implications for seismic hazard: San Francisco, California, American Geophysical Union, Fall meeting, abstract T43I-08.

Surpless, B.E., Stockli, D.F., Dumitru, T.A., and Miller, E.L., 2002, Two-phase westward encroachment of Basin and Range extension into the northern Sierra Nevada: Tectonics, v. 21, p. 2-1–2-10, doi:10.1029/2000TC001257.

Swan, F.H., 1988, Temporal clustering of paleoseismic events on the Oued Fodda fault, Algeria: Geology, v. 16, p. 1092–1095, doi:10.1130/0091-7613(1988)016<1092:TCOPEO>2.3.CO;2.

Thatcher, W., Foulger, G.R., Julian, B.R., Svarc, J., Quilty, E., and Bawden, G.W., 1999, Present-day deformation across the Basin and Range Province, western United States: Science, v. 283, p. 1714–1718, doi:10.1126/science.283.5408.1714.

Thompson, R.S., Benson, L.V., and Hattori, E.M., 1986, A revised chronology for the last Pleistocene lake cycle in the central Lahontan basin: Quaternary Research, v. 25, p. 1–9.

Unruh, J., Humphrey, J., and Barron, A., 2003, Transtensional model for the Sierra Nevada frontal fault system, eastern California: Geology, v. 31, p. 327–330, doi:10.1130/0091-7613(2003)031<0327:TMFTSN>2.0.CO;2.

Wallace, K., Yin, G.H., and Bilham, R., 2004, Inescapable slow slip on the Altyn Tagh fault: Geophysical Research Letters, v. 31, L09613, doi:10.1029/2004GL019724.

Wallace, R.E., 1977, Profiles and ages of young fault scarps, north-central Nevada: Geological Society of America Bulletin, v. 88, p. 1267–1281, doi:10.1130/0016-7606(1977)88<1267:PAAOYF>2.0.CO;2.

Wallace, R.E., 1987, Grouping and migration of surface faulting and variation in slip rates on faults in the Great Basin Province: Bulletin of the Seismological Society of America, v. 77, p. 868–877.

Ward, S.N., 1998, On the consistency of earthquake moment rates, geological fault data, and space geodetic strain: The United States: Geophysical Journal International, v. 134, p. 172–186, doi:10.1046/j.1365-246x.1998.00556.x.

Wernicke, B., and Snow, J.K., 1998, Cenozoic tectonism in the central Basin and Range: Motion of the Sierran–Great Valley block: International Geology Review, v. 40, p. 403–410, doi:10.1080/00206819809465217.

Wesnousky, S.G., 2005, Active faulting in the Walker Lane: Tectonics, v. 24, TC3009, doi:10.1029/2004TC001645.

Wesnousky, S.G., Bormann, J.M., Kreemer, C., Hammond, W.C., and Brune, J.N., 2012, Neotectonics, geodesy, and seismic hazard in the northern Walker Lane of western North America: Thirty kilometers of crustal shear and no strike slip?: Earth and Planetary Science Letters, v. 329–330, p. 133–140, doi:10.1016/j.epsl.2012.02.018.

White, N.J., Jackson, J.A., and McKenzie, D.P., 1986, The relationship between the geometry of normal faults and that of the sedimentary layers in their hanging walls: Journal of Structural Geology, v. 8, p. 897–909, doi:10.1016/0191-8141(86)90035-0.

Wong, I., and Olig, S.S., 1998, Seismic hazards in the Basin and Range Province: Perspectives from probabilistic analyses, *in* Lund, W.R., ed., Western States Seismic Policy Council, Basin and Range Province Seismic-Hazards Summit, Proceedings Volume: Utah Geological Survey Miscellaneous Publication 98-2, p. 110–127.

Wong, I., Silva, W., Olig, S., Thomas, P., Wright, D., Ashland, F., Gregor, N., Pechmann, J., Dober, M., Christenson, G., and Gerth, R., 2002, Earthquake scenario and probabilistic ground shaking maps for the Salt Lake City, Utah, metropolitan area: Utah Geological Survey Miscellaneous Publication MP-02-05, 50 p., with CD-ROM.

Wong, I., Olig, S., Dober, M., Silva, W., Wright, D., Thomas, P., Gregor, N., Sanford, A., Lin, K., and Love, D., 2004, Earthquake scenario and probabilistic ground-shaking hazard maps for the Albuquerque–Belen–Santa Fe, New Mexico corridor: New Mexico Geology, v. 26, p. 3–33.

Zreda, M., and Noller, J., 1998, Ages of prehistoric earthquakes revealed by cosmogenic chlorine-36 in a bedrock fault scarp at Hebgen Lake: Science, v. 282, p. 1097–1099, doi:10.1126/science.282.5391.1097.

Science Editor: Christian Koeberl
Associate Editor: Clinton Conrad

Manuscript Received 2 July 2014
Revised Manuscript Received 14 October 2014
Manuscript Accepted 3 November 2014

Printed in the USA